Electrochemical Impedance Spectroscopy for Battery Research and Development

Technical Report 31

Electrochemical Impedance Spectroscopy for Battery Research and Development

Technical Report 31

Dedicated to George Feldman

Dr. Hong Shih
Cortech Corporation
P.O. Box 92254
City of Industry
California
CA91715-2254
U.S.A.

Dr. Tai-Chin Lo
Department of Electrical and Electronic Engineering
The Hong Kong University of Science and Technology
Clear Water Bay
Kowloon
Hong Kong

For details of our agents in other countries, please contact our Farnborough, UK office.

Solartron Instruments pursue a policy of continuous development and product improvement. The specification in this document may therefore be changed without notice.

Electrochemical Impedance Spectroscopy
for Battery Research and Development

Dedicated to George Feldman

Dr. Hong Shih
Cortech Corporation
P.O. Box 92254
City of Industry
California
CA91715-2254
U.S.A.

Dr. Tai-Chin Lo
Department of Electrical and Electronic Engineering
The Hong Kong University of Science and Technology
Clear Water Bay
Kowloon
Hong Kong

Index

1. Introduction

Electrochemical techniques are very helpful for evaluation of batteries and cells during charge and discharge, and in service, as the nature of chemical and electrochemical processes occurring in these devices may be determined.   Both traditional and an accelerated screening test method are necessary to analyse and compare battery properties, to obtain kinetic information, and to predict the likelihood of failure.

In comparison with dc electrochemical techniques, electrochemical impedance spectroscopy (EIS) has great advantages. EIS can not only provide detailed kinetic information, but can also be used to monitor changes in battery properties under different usage or storage conditions. EIS is a very sensitive technique, and offers a wealth of information about battery systems such as :

- analysis of state of charge
- study of reaction mechanisms
- change of active surface area during operation
- separator evaluation
- passivating film behaviour
- separation and comparison of electrode kinetics on each electrode
- identification of possible electrode corrosion processes
- investigation of the kinetics at each electrode

Since the perturbating ac signal is very small, the resultant polarisation of the electrode is in a linear potential region. Therefore, there is no destructive damage to the electrode, and EIS can be used to evaluate the time relation of interface parameters. Due to the great advantages of electrochemical impedance spectroscopy, this technique is now widely applied to the study of batteries and fuel cells. There is also a growing interest in solid, ionically conducting polymers as potential battery electrolytes due to their advantageous mechanical properties, ease of fabrication as thin films and their ability to form a good contact with electrode materials.

Applications of EIS have included starting, lighting and ignition (SLI) and electric vehicle (EV) batteries, fuel cells, and solid-state batteries such as polymer electrolyte batteries, as described in a number of technical papers and conference symposia. In the proceedings of the symposium on electric vehicles, Halpert (1) has

summarized and compared commonly used advanced batteries for electric vehicle application, and discussed specifications, suitability, risk, and likelihood of success for each type. Solid state batteries and their specifications were also reviewed by Squire (2) in this symposium. Selman and Lin (3) have detailed the application of ac impedance testing for fuel cell research and development.

This monograph presents a detailed description of the current application of EIS to battery study and development.

2.   Electrochemical Impedance Spectroscopy (EIS)

Electrochemical Impedance Spectroscopy (EIS) has many advantages in comparison with other electrochemical techniques. During EIS experiments, a small amplitude ac signal is applied to the system being studied. EIS is a non-destructive method for the evaluation of a wide range of materials, including coatings, anodized films, corrosion inhibitors, batteries and fuel cells, and can provide detailed informaton of the systems under examination; parameters such as corrosion rate, electrochemical mechanisms and reaction kinetics, detection of localized corrosion, battery life and fuel cell performance can all be determined from these data.

In common corrosion studies, such as coatings evaluation or corrosion rate measurement, EIS experiments are usually performed with the applied dc potential (called dc bias) equal to the corrosion potential (open circuit potential).   In EIS studies of battery systems, the dc bias is applied at different potentials in order to investigate the corrosion or kinetic processes taking place during charging or discharging. EIS may be performed in either potentiostatic (constant voltage) or galvanostatic (constant current) mode depending on the type of analysis.

2.1   Experimental Techniques

The electrical impedance of an electrocehmical cell can be measured either directly with an Impedance Analyser such as the Solartron model 1260A, or with a combination of a Frequency Response Analyser (FRA) and an electrochemical interface (ECI), such as the Solartron 1255A and 1287A units. The ECI is an high-bandwidth potentiostat which provides the dc cell bias voltage or current, and a small sinusoidal ac signal (typically a few millivolts) from the FRA is superimposed.

The ac response from the cell over a range of applied frequencies is analysed by the FRA and the impedance is calculated. A common hardware configuration is shown in Fig. 1.
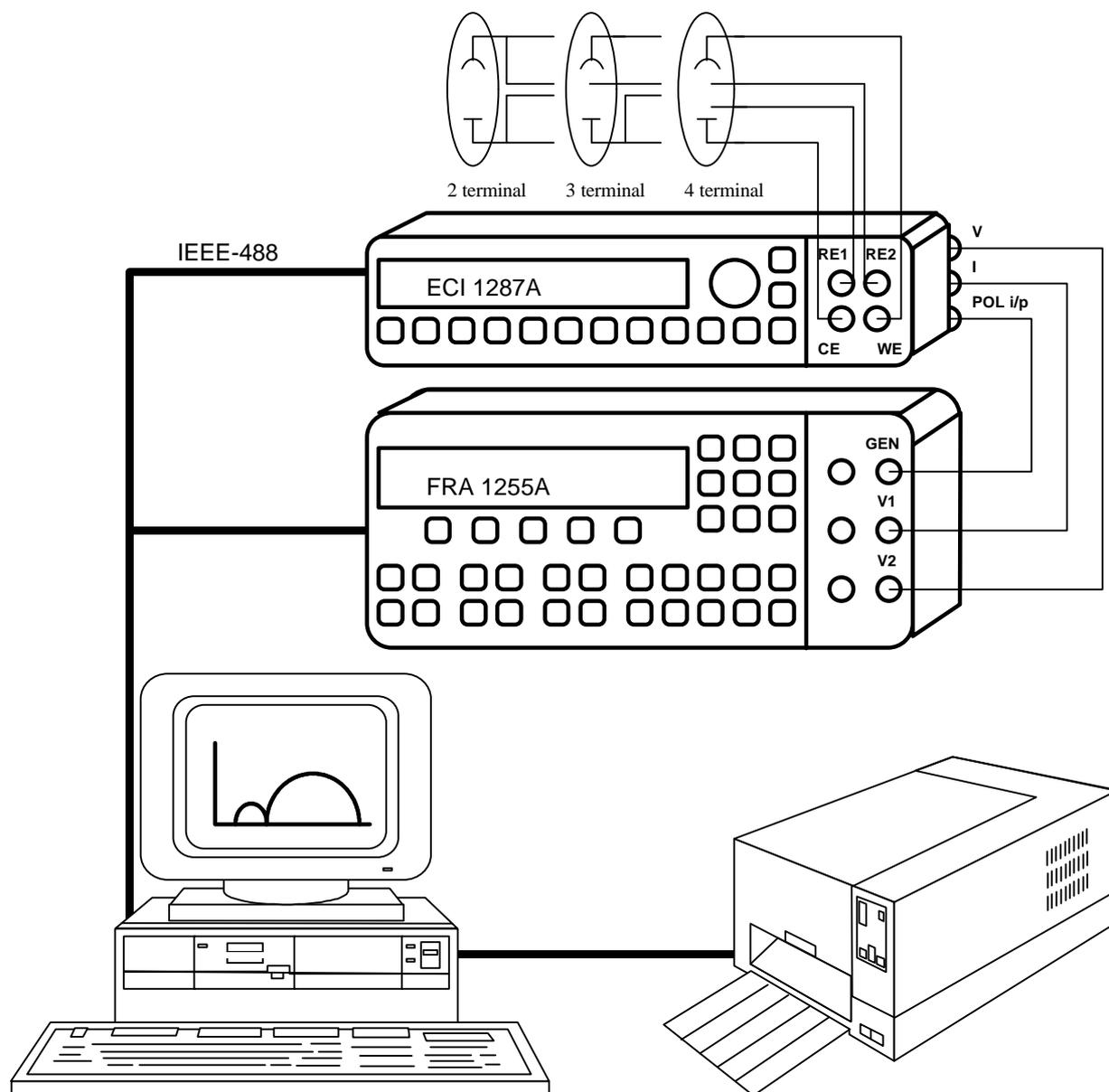
Fig. 1 EIS measurement and data acquisition system

Data collection, display and analysis is normally controlled by software running on a personal computer (4,5). Equivalent circuit modelling has been accepted as the means of interpreting electrochemical impedance results (6), as this offers a convenient way of analysing and investigating changes in cell behaviour. Other publications describe the theory, experimental practice and interpretation in more

detail (7-10).   Results are plotted in the complex plane (Nyquist plot) or as magnitude and phase versus frequency (Bode plot).
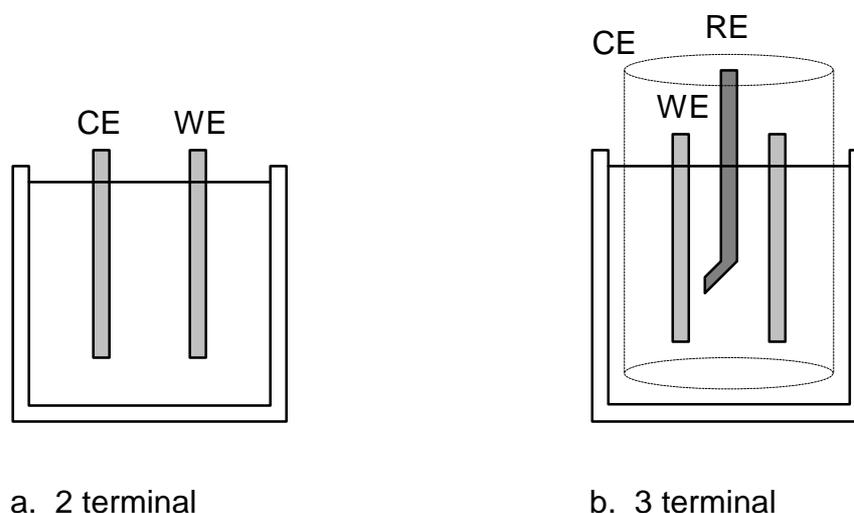

a. 2 terminal   b. 3 terminal

Fig. 2 Cell configurations

Batteries may be analysed in either a 2-terminal or 3-terminal configuration. Typical cell designs are shown in Fig. 2. The 2-terminal connection is utilised to test the behaviour of a whole cell or battery; for 3-terminal measurements, a reference electrode is introduced in order to measure the reactions at each individual electrode. In this case, a cylindrical mesh is often used as counter electrode in order to avoid errors due to polaristion of the other battery electrode, or any risk of damage due to excessive current density.

The following sections will describe different applications of EIS for analysis of a range of battery systems and fuel cells.

3.   Lead-Acid Batteries

The most popular batteries used in automobile industry are lead-acid batteries. From the first work by Gaston Plante in 1859, flooded lead/acid batteries were the workhorse in the portable energy field for the 100 or so years following their inception. Although many significant improvements and modifications were made over the years, the basic technology for flooded lead/acid chemistry/technology remained intact. The 1989 international conference on lead-acid batteries covered

most information of the recent development and applications of lead-acid batteries (11). Reported improvements were directed toward enhancements in energy density, cycle life, high rate discharge performance, processing and materials such as separators and grids (11-51). Nelson (12) pointed out that the two fundamental drawbacks of flooded lead/acid batteries were the heavy gassing levels on overchar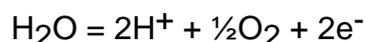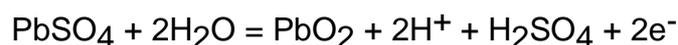ge and their tendency to leak electrolyte. In 1912, Thomas Edison was issued a patent (52), whereby he demonstrated that gases could be retained within a battery via combustion using a heated platinum element. Tichenor (53) augmented the platinum approach by using auxiliary electrodes. In 1938, Dassler (54,55) was issued two patents that specifically addressed the recombination of H_2 and O_2 gases in alkaline or lead/acid secondary cells.

The development of nickel/cadmium (Ni/Cd) cells based upon oxygen-recombination principles through Neumann and Gottesmann (56) also provided help in the development of lead/acid batteries; the so called "supported active materials" approach by Szper, the gel technology by Vinal (57), by Eberts and Jache (58,59), and by Sonnenschein and Johnson Controls. With the development of sealed gas-recombination lead/acid batteries, these were first introduced into automobiles in Australia in the late 1970s. Since then, their use has been extended to South Africa, U.S.A., and later to Europe. Recently, lead/acid batteries have found more applications in automobile industry (37-42). The principles of oxygen cycle and gas recombination in a lead/acid cell are shown as follows:
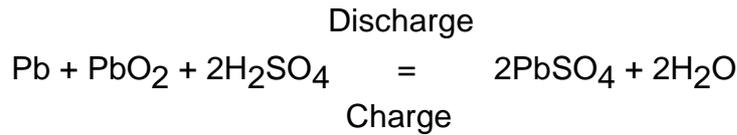
At the negative plate:

$$PbSO_4 + 2e^- + 2H^+ = Pb + H_2SO_4$$

$$2H^+ + 2e^- = H_2$$

At the positive plate:

$$PbSO_4 + 2H_2O = PbO_2 + 2H^+ + H_2SO_4 + 2e^-$$
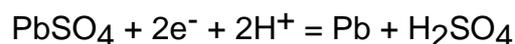
$$H_2O = 2H^+ + \tfrac{1}{2}O_2 + 2e^-$$

The overall process is shown below:

$$\text{Discharge}$$
$$Pb + PbO_2 + 2H_2SO_4 \quad = \quad 2PbSO_4 + 2H_2O$$
$$\text{Charge}$$

The recombination reaction:

$$Pb + \tfrac{1}{2}O_2 + H_2SO_4 = PbSO_4 + H_2O$$

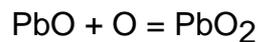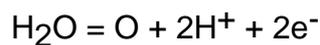## 3.1   Grid Corrosion

The grid corrosion of the positive plate has become a very important issue for the life time of lead/acid batteries. Investigations have involved the study of grid materials, design of the optimum grid geometry, the evaluation of the corrosion processes on the grid during charge/discharge processes, and the development of an accelerated test for screening positive grid materials used in lead/acid batteries. Positive plate corrosion is the major cause of failure in lead/acid batteries, but from time to time an abnormal corrosion of negative grid lugs was observed. The corrosion is due to the presence of H_2O at the Pb surface and diffusion of oxygen through the crystal lattice as shown below:

$$Pb + H_2O = PbO + 2H^+ + 2e^-$$

$$H_2O = O + 2H^+ + 2e^-$$

$$PbO + O = PbO_2$$

$$PbO + mPbO_2 \rightarrow PbO_n$$

The grid corrosion is controlled by the transport of oxygen through the inner corrosion product layer, and the morphology and structure of this layer is important for cyclic operation. In order to develop an accelerated test for screening positive grid materials used in the lead acid batteries, Ying, Wang, and Garabedian (42) have studied the corrosion of Pb and positive grid electrodes by cyclic voltammetry and EIS. They concluded that cyclic voltammetry revealed only slight differences in the corrosion behavior between the pure lead and the production grid alloy. However, distinct differences in impedance parameters were observed for these two materials. Physically significant equivalent circuit models have been proposed to

describe the structural and kinetic changes during charging and discharging of the electrodes.
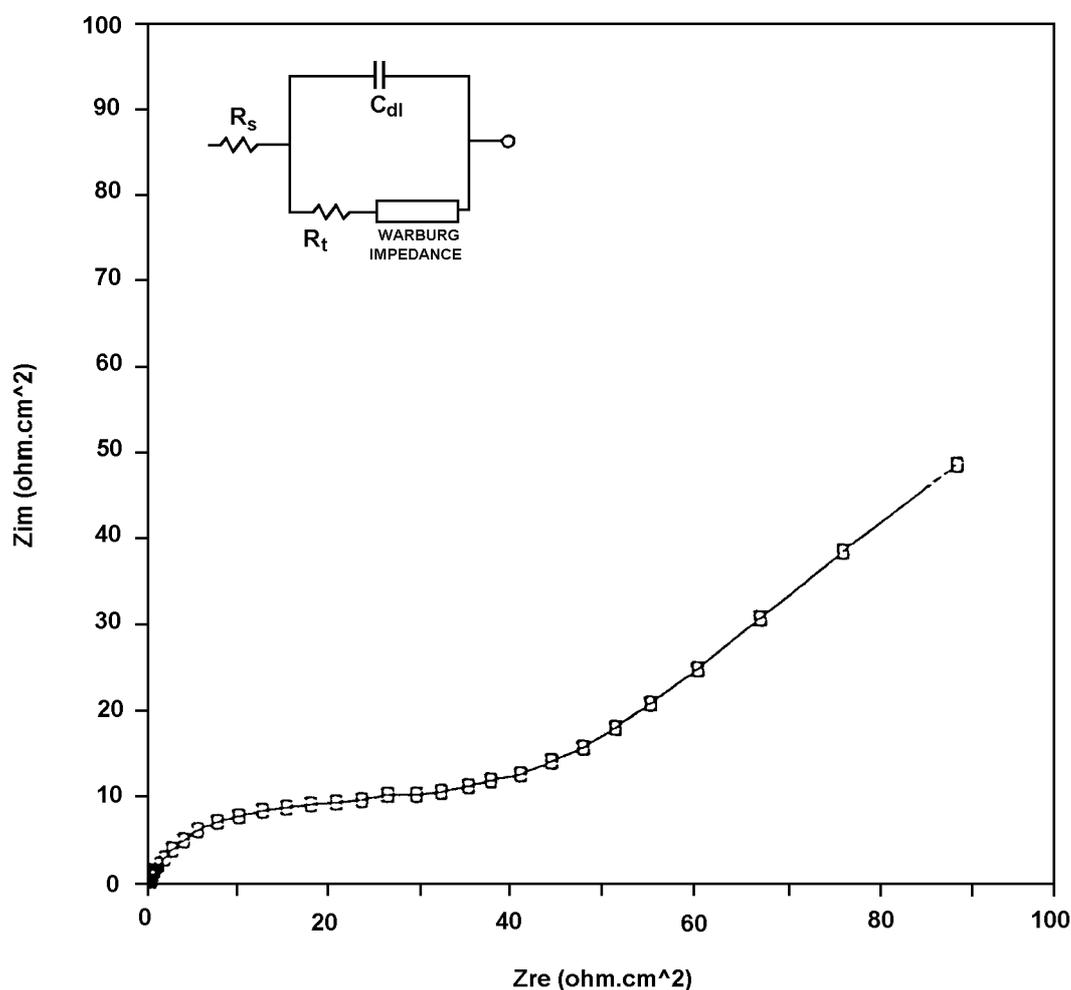
Fig. 3 The Nyquist plot for pure Pb at the Pb/PbSO$_4$/5M H$_2$SO$_4$ equilibrium potential (42)

Experimental studies utilised a Solartron 1250 frequency response analyzer coupled with a potentiostat with a sinusoidal perturbation voltage of 5 mV rms. Hg/Hg$_2$SO$_4$ was used as the reference electrode (0.609 V SHE). Fig. 3 shows a Nyquist plot of pure lead in 5M H$_2$SO$_4$ solution at the equilibrium potential (-0.960 V). The impedance spectra indicate a charge transfer resistance (R$_t$) and a mass transport component (Warburg impedance, W) in parallel with a double layer capacitance (C$_{dl}$) (47). R$_t$ is calculated as 23 ohm.cm², and C$_{dl}$ is 113 µF/cm², which is in good

agreement with the value reported by Armstrong and Bladen (48). For the alloy grid, a similar impedance behavior was observed; however R_t is smaller (6 ohm.cm²) indicating that the corrosion rate of lead alloy is higher than that of pure lead at the $Pb/PbSO_4$ equilibrium potential.

During potentiostatic charging, a conducting PbO_2 layer was formed on the Pb surface. The anodic currents were contributed by two reactions:

$$Pb + 2H_2O \rightarrow PbO_2 + 4H^+ + 4e^-$$

$$2H_2O \rightarrow O_2 + 4H^+ + 4e^-$$
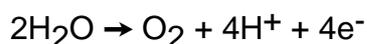
A porous Pb oxide was formed during charging, the increasing capacitance with charging time indicated that the active surface area of the PbO_2 layer was increasing. A pseudocapacitance was reported by Maja and Penazzi (49). To a certain time limit, the product of R_tC_{dl} remained constant and the reaction of oxygen evolution was the dominant reaction. A typical Bode-impedance and Bode-phase angle plots for the pure lead electrode at 1.4 V were shown in Fig. 4. A Randles-type impedance spectrum was observed.
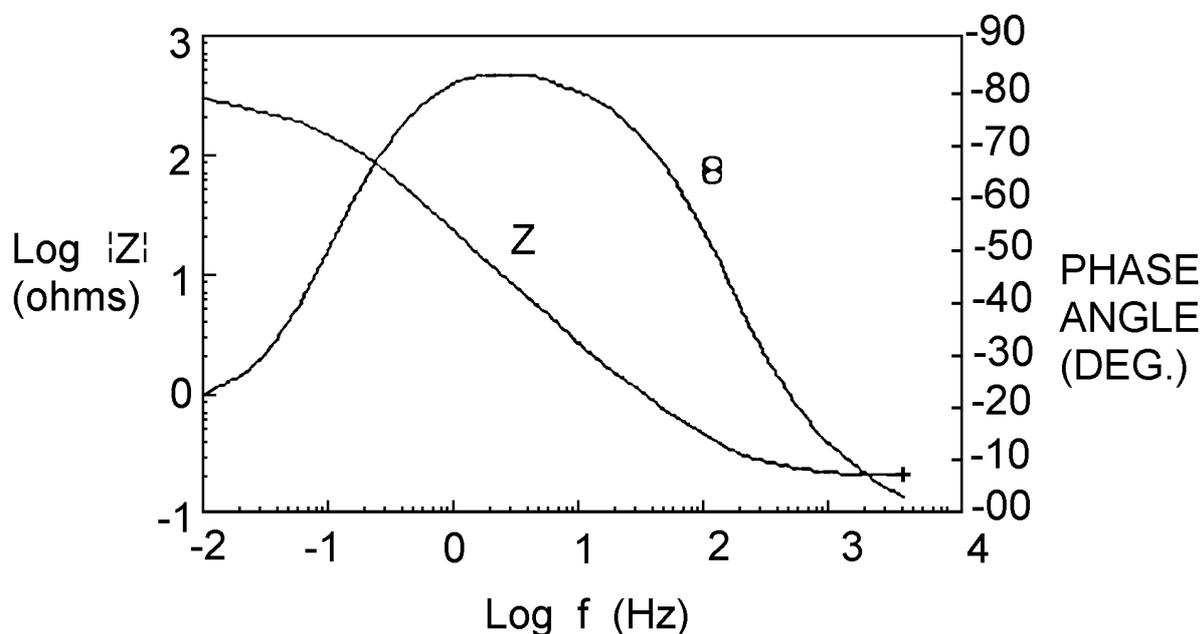
Fig. 4 Bode plots for pure Pb charged at 1.4 V for 20 hours (42)
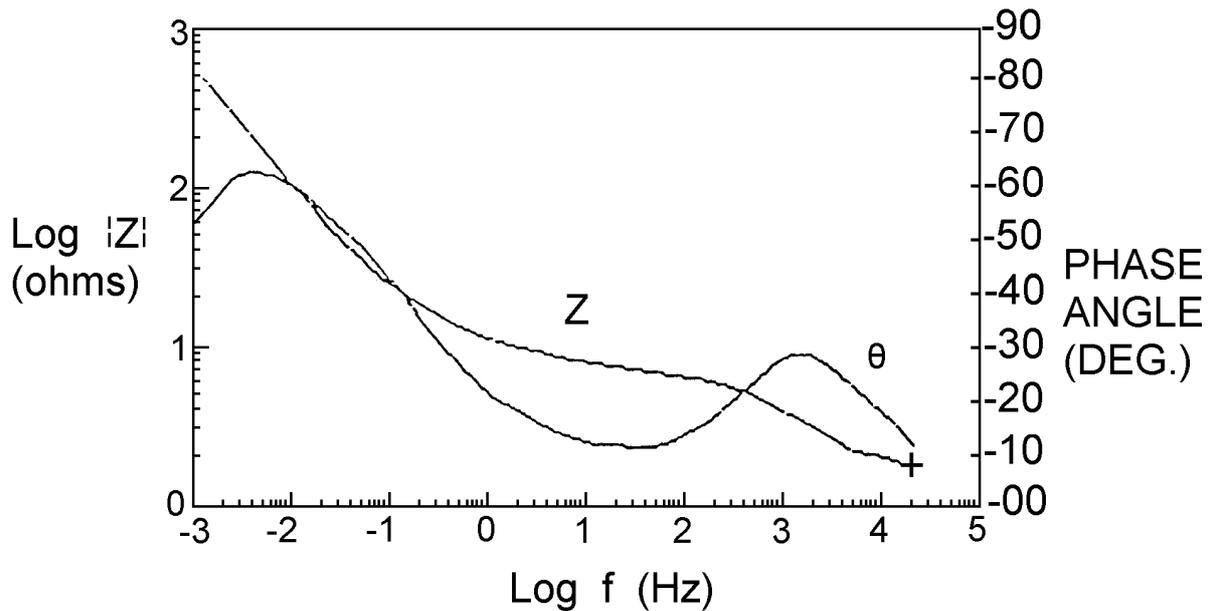
Fig. 5 Bode plots for pure Pb electrode potentiostatically discharged at 0.93 V for 5 hours. The electrode was previouly charged at 1.4 V for 164 hours (42)

After charging, the electrode remained at open circuit voltage (OCV) for 30 minutes, and the open circuit potential was about 1.160 V. By holding at 0.930 V, a very high cathodic (discharge) current was observed. EIS measurements were carried out at this potential. The impedance spectra showed a two time constant model plotted in Fig. 5. The interface model can be described by the coating model shown in Fig. 6 with or without Warburg impedance at the low frequencies.
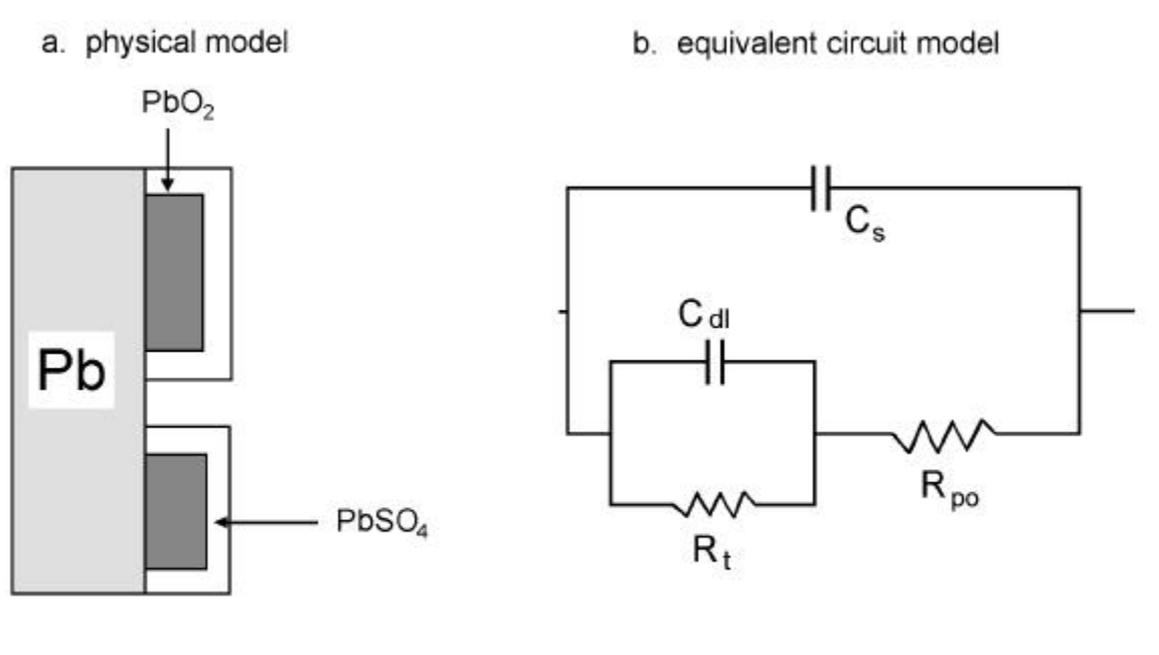
Fig. 6 Models for a discharged PbO$_2$ electrode (42)

Although the impedance spectra of the pure Pb electrode and the grid alloy are similar, the value of R_t for the Pb electrode is much higher than that of the grid alloy. The $PbSO_4$ layer formed on Pb electrode is more protective than that formed on the Pb alloy electrode.

Wang and coauthors have carried out measurements of lead-acid gas recombination batteries on the EV program. Three and two electrode systems have been applied in the measurements. For a three electrode system, both positive and negative electrodes were measured separately in order to obtain the kinetics on each electrode. For a Pb grid alloy, the positive electrode showed a one-time constant model with a typical impedance spectra of Fig. 7, recorded after 300 cycles and obtained in 5M H_2SO_4.
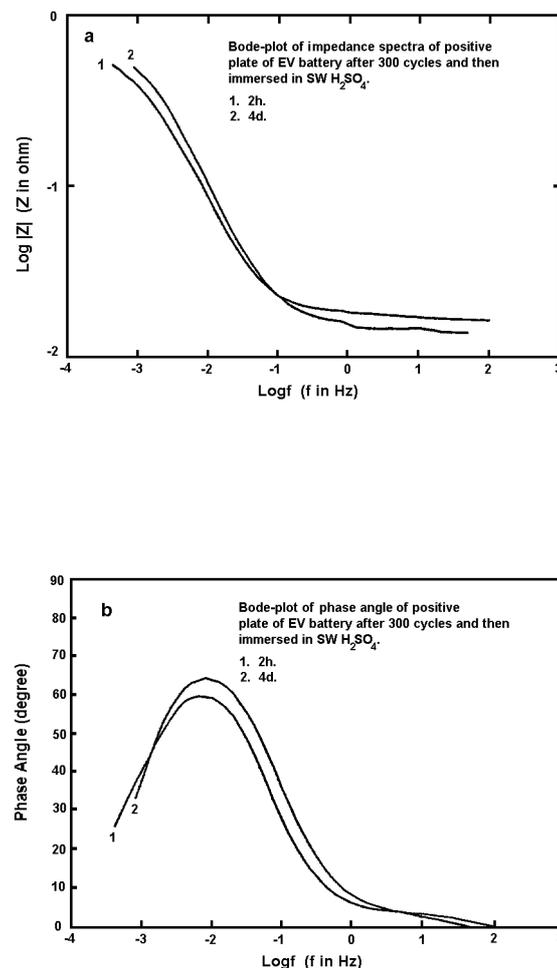
Fig. 7 Bode plots of positive plate of lead-acid battery after 300 cycles and then immersed in 5M H_2SO_4 (41)
1. 2hours   2. 4days
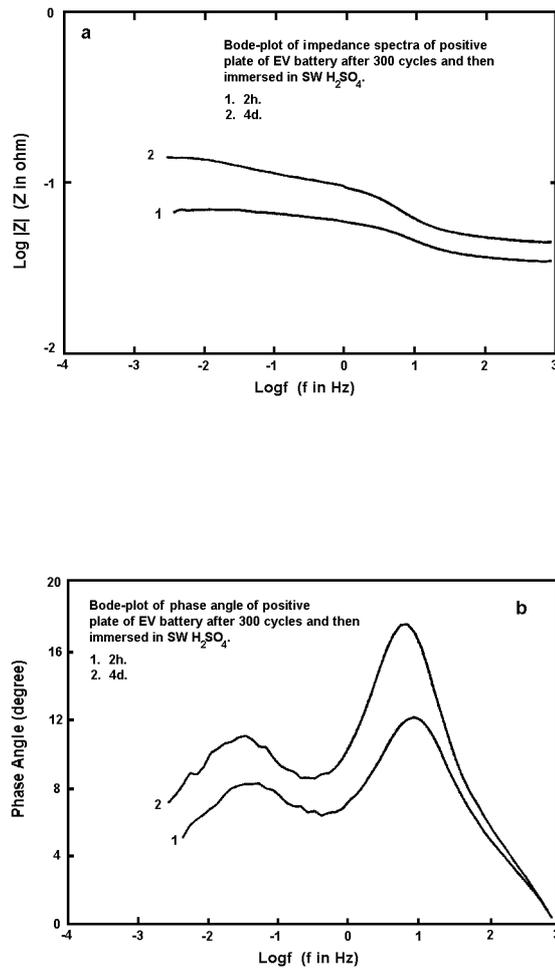
Fig. 8 Bode plots of negative plate of lead-acid battery after 300 cycles and then immersed in 5M H$_2$SO$_4$ (41)
1. 2hours   2. 4days

For the negative plate after 300 cycles, the impedance spectra are shown in Fig. 8, where a two-time constant model was observed. Sometimes, a Warburg impedance was obtained during EIS measurements. The two-electrode system always provided a two-time constant model with or without a Warburg impedance at the low frequencies.

The typical results for the lead-acid battery after 300 cycles measured at E_{cell} using a three electrode system in 5M H$_2$SO$_4$ are listed in Table I.

Table I - Interface parameters of lead-acid battery after 300 cycles

Electrode	Time	R_s (W)	R_1 (W)	R_t (W)	C_1 (F)	C_{dl} (F)	a_1	a_2	E_{cell} (V)
Positive plate	2hours	0.017	-	0.565	-	268	-	0.875	2.15
Positive plate	4days	0.015	-	0.585	-	213	-	0.905	2.17
Negative plate	6hours	0.030	0.025	0.015	1.2	140	0.75	0.95	2.15

The negative plate showed a two time-constant model with low internal resistance, but the positive plate had much high internal resistance. Charge transfer resistance R_t increased from 0.565 ohm to 0.585 ohm, and the double capacitance C_2 decreased from 268 farad to 213 farad after 4 days operation. This indicates the loss of active surface area on the positive plate under certain assumptions and the increase of internal resistance. The increase of internal resistance may be due to the formation of corrosion products.

From the EIS results, the following conclusions can be obtained:

- After charging and during cycling, the overall impedance of a lead-acid gas recombination battery showed a two time-constant model with or without Warburg impedance.

- The time constant occurring at the high frequencies was only due to the reaction at the negative plate.

- The negative plate had a small value of R_t and had very small influence on the failure of the battery.

- For the positive plate, EIS showed a one time-constant model with or without a mass transport effect. Following the changes of R_t and C_{dl} with time, it is possible to estimate the loss of active surface area, the increase of internal resistance, the effect of mass tranport, the property of the separators, and the failure of the plate.

- For the positive electrode during charging, EIS showed a one time constant model with Warburg impedance. C_{dl} increased with charging time and R_t increased to a maximum and then decreased, but the $R_t C_{dl}$ product remained constant after a certain charging time.

## 4.	Lithium-Titanium Disulfide Rechargeable Cells

Among the several high energy rechargeable lithium battery systems based on lithium-intercalatable cathodes (60), the one using TiS_2 has been advanced to a status of significant technological development. The Li/TiS_2 cell consists of an elemental lithium anode (negative electrode), a titanium disulfide cathode (positive electrode), and a lithium salt dissolved in an aprotic nonaqueous solvent as the electrolyte. During discharge of the cell, lithium ions intercalate in the TiS_2 cathode forming Li_xTiS_2 (0 < x < 1), and elemental lithium at the anode is oxidized to lithium ions. These cells can be charged and discharged between 1.6 V and 2.7 V. Specific energy values in the range of 75 to 100 Wh/kg and 300 to 500 charge/discharge cycles have been realized (61-64). Recently, Narayanan and coauthors (65) have studied Li/TiS_2 cell by EIS; the impedance of these rechargeable cells as a function of frequency, state of charge, and extended cycling have been evaluated. The kinetic parameters for the various processes occurring at the electrode/electrolyte interface and the causes of cell degradation and failure during extended cycling have been investigated by EIS and evaluated by equivalent circuit modelling (65).

The two-terminal impedance of the Li/TiO_2 cells was measured between 10 mHz and 65 kHz using a Solartron Frequency Response Analyzer 1255 interfaced with a potentiostat/galvanostat controlled by an IBM PS/2 computer. The sinusoidal excitation voltage applied to the cells was 2 mV rms. Under these conditions, the ac test currents did not exceed 100 µA cm^{-2}. Thus the level of sinusoidal perturbation of 2 mV rms ensured a linear steady-state response. For the measurements at various states of charge, the cells were charged to the chosen level and allowed to stand at the open-circuit cell voltage for 24 hours. After this period, the open-circuit cell voltage attained an equilibrium value with a variation of 100 µV/h, which was considered adequate as an equilibrium state for the ac impedance measurements.

The typical impedance spectra reflecting the state of charge are shown in Fig. 9. The impedance spectra showed a two time-constant model with a dominant

Fig. 9 Typical impedance response of Type A cells at various open-circuit voltages, state of charge shown by value of X (74)

Warburg impedance at the low frequencies. For cells subjected to over 600 cycles, the impedance spectra showed a one time-constant model with a low frequency Warburg impedance as shown in Fig. 10.
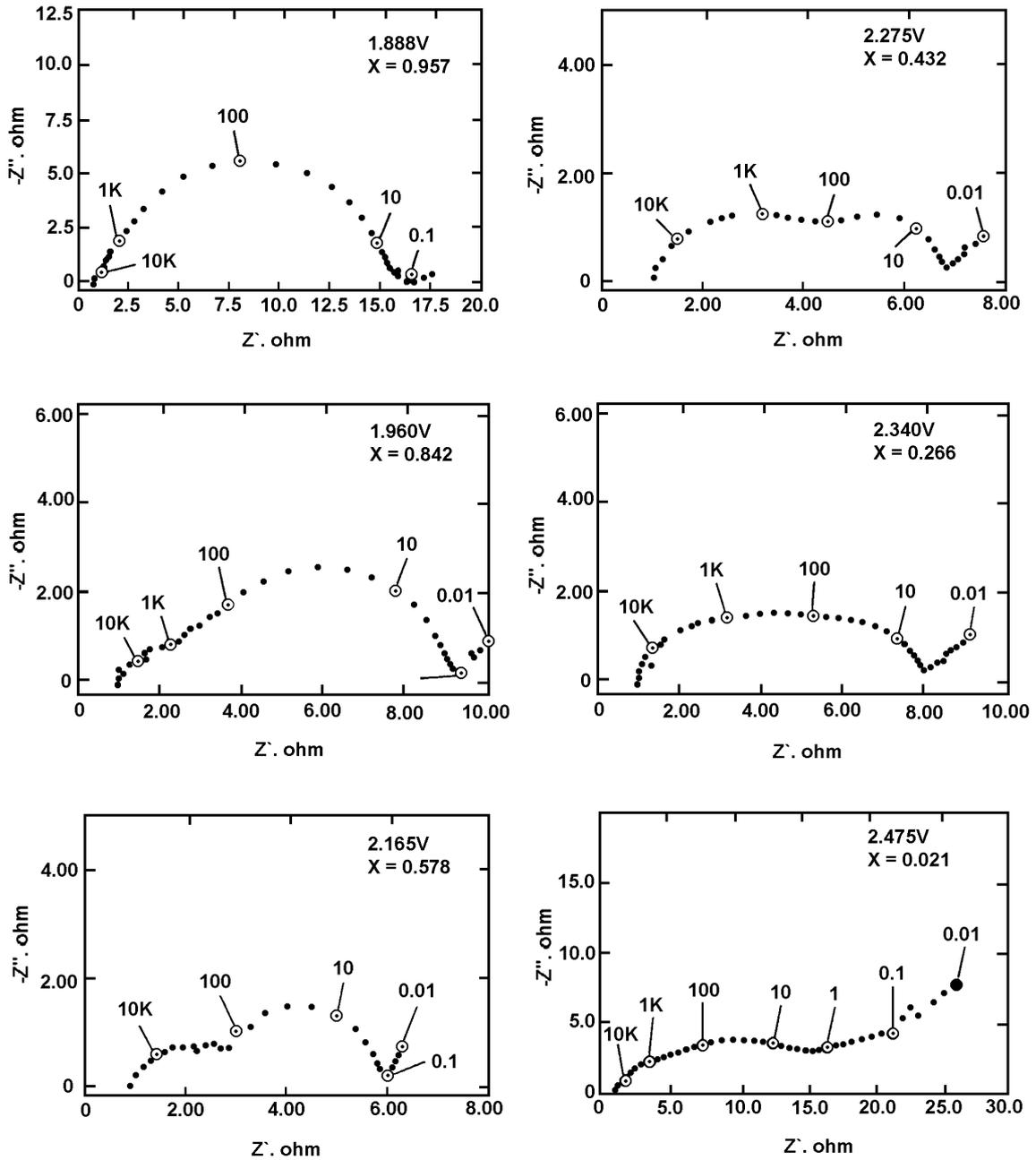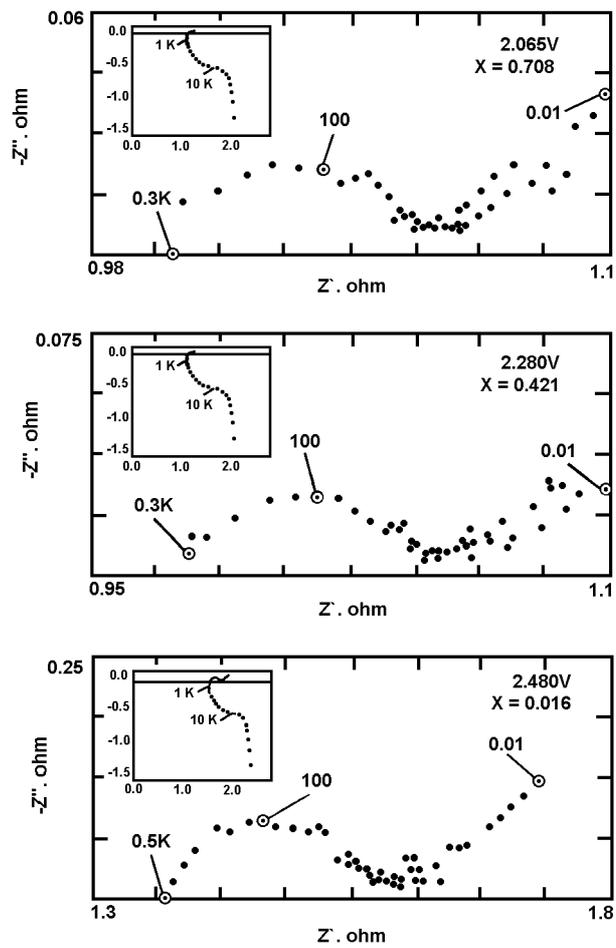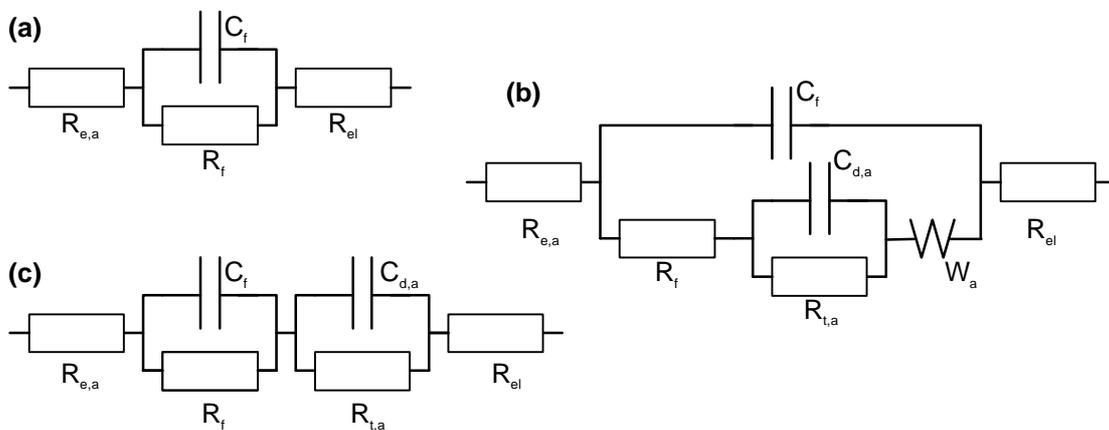
Fig. 10 Typical impedance response of Type B cells at various open-circuit voltages (state of charge given by value of X). Insets show response in the range 1 to 60 kHz (74)

Possible equivalent circuits of the Li/solution interface were suggested as follows:

In these models, R_f and C_f are the resistance and capacitance of the passivating surface film, respectively; $R_{t,a}$ and $C_{d,a}$ are the charge transfer resistance and double layer capacitance of the anode, respectively; W_a is the Warburg impedance of electroactive species; $R_{e,a}$ is the contact resistance; and R_{el} is the resistance of the electrolyte. Model (a) is the simplified one time-constant model which is in general agreement with the literature (66,67).

For the TiS$_2$/solution interface, the equivalent circuit was suggested as follows:
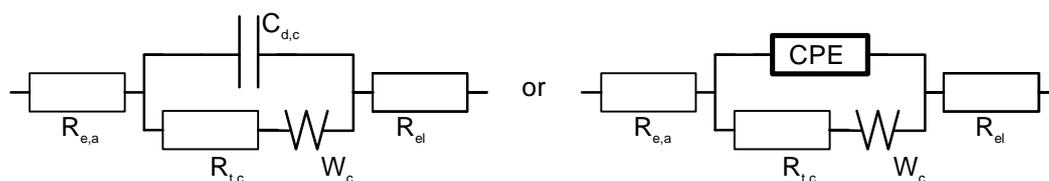
where $R_{t,c}$ and $C_{d,c}$ are the charge transfer resistance and double layer capacitance of the cathode respectively, W_c is the Warburg impedance, and CPE is the constant phase element due to the rough or porous surface of the electrode. The charge-transfer equilibrium at the cathode is

$$x\,Li^+ + TiS_2 + xe^- = Li_xTiS_2$$
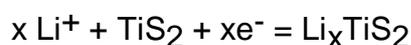
Under the condition of the ac impedance measurements, the linearized Butler-Volmer relation applied, and $R_{t,c} = (RT/nFi_{o,c})$, where $i_{o,c}$ is the exchange current at the cathode.

Fig. 11 Plot of charge transfer resistance at the cathode vs. $\{x(1-x)\}^{-1/2}$ (74)

A linear relation between $R_{t,c}$ and $1/\{x(1-x)\}^{1/2}$ was observed, shown in Fig. 11, which is consistent with the expression as follows:

$$R_{t,c} = \{RTV_m/n^2F^2Ak^oC^{1/2}\,Li^+\}\{x(1-x)\}^{1/2}$$
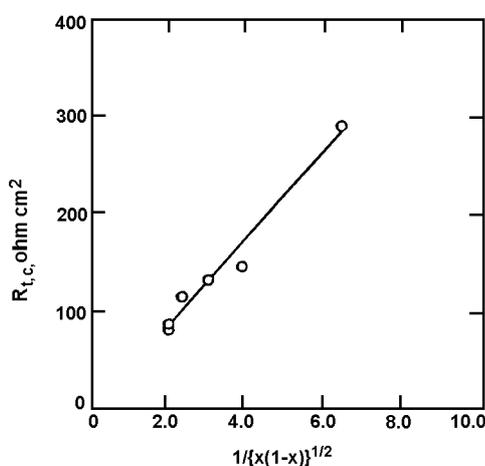
Using a complex nonlinear least square method developed by Boukamp (68,69), the interface parameters were analyzed for Li/TiS$_2$ cells after 5 and 600 cycles. The following conclusions can be drawn:

- A dramatic increase of ohmic resistance, which is the sum of electrodes, electrolyte, and the separator, was observed after extended cycling.

- The charge-transfer resistance and lithium-ion diffusion in the solid matrix of the cathode are not significantly affected.

- The impedance response showed extensive morphological change and area enhancement occurred at the anode.

- EIS can be used to identify the effect of extended cycling on the various physiochemical processes occurring in the Li/TiS$_2$ cell.

5.   Li/Li$_x$MnO$_2$ Cells

The impedance of Li electrodes in different electrolytes for Li accumulators has been studied by various authors (70-74). The main objectives were to find out the correlation between the impedance parameters and the cycling efficiency of the Li electrode. A general interface model was applied in these papers. It was analogous to the one used for passivated Li in some of electrolytes for primary Li cells, such as LiSOCl$_2$ (75-77), Li/SO$_2$ (78,79), and Li/PC (79). Recently, Bojinov and coauthors (80) have studied the impedance of Li electrode in Li/Li$_x$MnO$_2$ accumulators at open circuit voltage (OCV). These studies were to collect more information about Li electrodes under real operating conditions, with the practical electrolyte commonly used, such as PC/EC (80-82), THF/2-MeTHF (83), 2-MeTHF/EC (84), all with LiAsF$_6$.
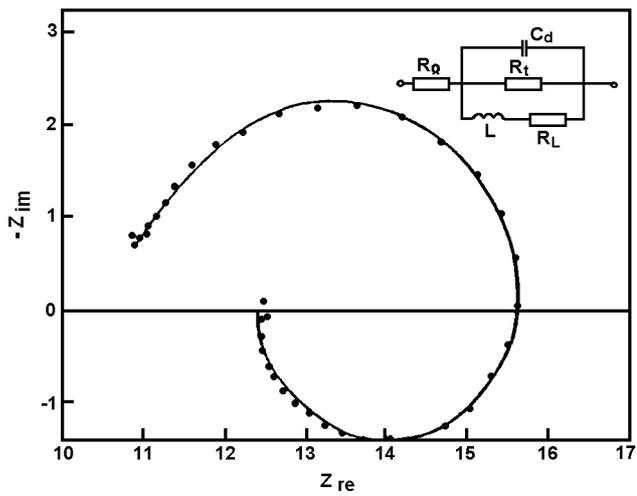
Fig. 12 Nyquist plot of a charged Li electrode in a Li/Li$_X$MnO$_2$ accumulator with electrolyte after 24 h at open circuit potential (80)
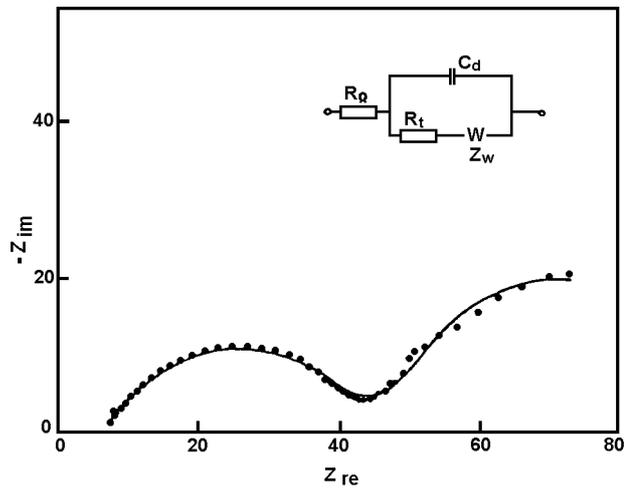

Fig. 13 Nyquist plot of an overcharged Li electrode in a Li/Li$_X$MnO$_2$ accumulator (80)
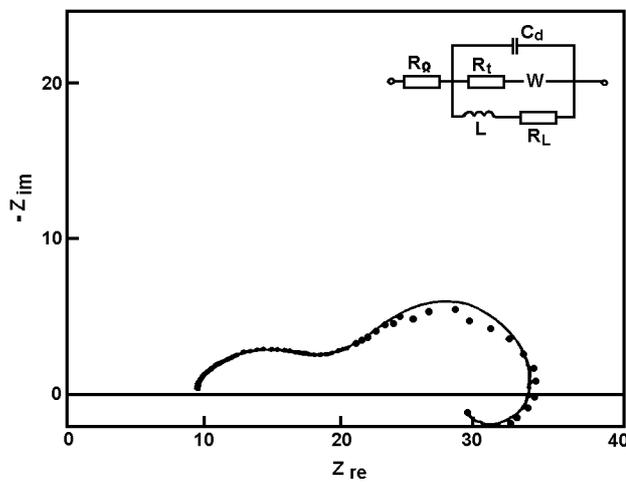

Fig. 14 Nyquist plot of the overcharged Li electrode after 1.8 C charge (80)

The impedance measurements were carried out in stainless steel laboratory cells. The construction of the cell and the preparation of the electrolytes are shown elsewhere (80). Cycling was performed galvanostatically in the limited voltage mode by a special computerized facility. The cycling regime was $i_c=i_d=1$ mA.cm^{-2}, U_{max} = 3.5 V, U_{min} = 1.8 V.

A Solartron 1250 frequency response analyzer coupled with a SI1286 electrochemical interface was used for the impedance measurements. The frequency was normally from 65 kHz to 1 mHz. The ac impedance measurements were performed at open circuit voltage in galvanostatic mode with an ac current amplitude of 10 µA. In order to reach the steady-state condition, impedance measurements were carried out 45-60 minutes after the cycling was completed. Fig. 12 shows a typical impedance plot of the Li electrode in a Li/Li$_x$MnO$_2$ cell in 1.5M LiAsF$_6$/THF/2MeTHF (1:1)/0.5% 2MeF for the 20th charge (U_{max} = 3.5 V). The first loop at high frequencies is characteristic of the charge transfer process at the Li/electrolyte interface (70-78). A second inductive loop at low frequencies corresponds to the relaxation process involving adsorbed intermediates.
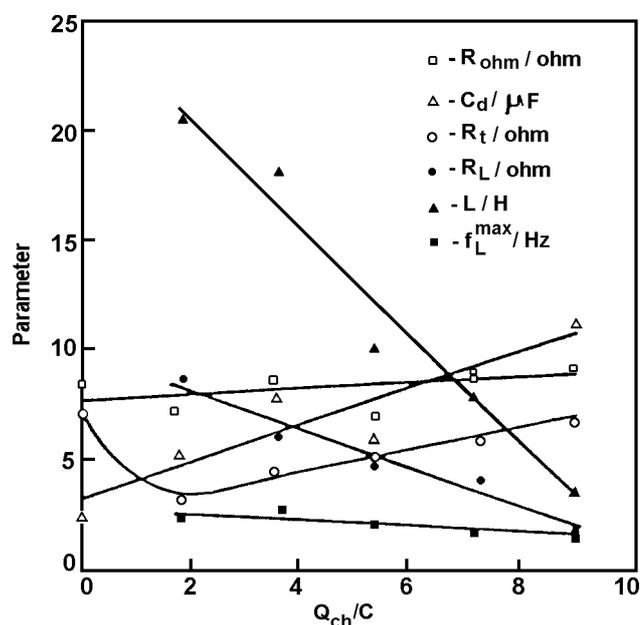

Fig. 15 Dependence of the equivalent circuit elements (Fig. 14) on the quantity of charge passed (80)

The impedance plot of an overcharged Li/Li$_x$MnO$_2$ cell, initially below 1.8 V, after 4 hours at a current of 0.5 mA cm^{-2} is shown in Fig. 13. The inductive loop disappears

after 1.8 C cm^{-2} of discharge and a low frequency diffusion (Warburg) impedance is observed. After a charge of 1.8 C cm^{-2}, the impedance spectrum is shown in Fig. 14; the inductive behavior is restored, but the Warburg impedance remains. The dependence of the equivalent circuit elements from Fig. 14 on the quantity of charge passed is plotted in Fig. 15. The anodic and cathodic reactions of the cells are listed below:

Anodic reaction : $Li \rightarrow Li^+ + e$

Cathodic reaction :   solvent + e $\rightarrow$ degradation products

A low-frequency inductive behavior was observed in the impedance spectra for various metals during their deposition/dissolution in aqueous electrolytes, e.g., iron dissolution in acidic and weak acidic solutions, Zn deposition in alkaline solution (85), Ni deposition from acid solvents (86), Al anodic oxidation (87,88), etc. A number of basic reasons for this behavior were proposed: (i) adsorption/desorption of intermediates (85-95); (ii) space charge relaxation (96); and (iii) dynamic system analysis based on an appropriate physical model of the iron dissolution mechanism (86-95). Another possibility of inductive behavior was mentioned by Chechirlian et al (97).

6.   Ni(OH)$_2$/NiOOH Electrodes

Macdonald (98) and coauthors have applied EIS as the principal experimental tool in this study. The degradation of porous nickel battery electrodes in alkaline media upon cyclic charging/discharging was studied. Macdonald et al developed a transmission line model (TML) for the impedance of the porous mass. The model was adopted from Lenhalt et al and Park and Macdonald (99), and considered the finite thickness of the electrode and assumed a finite resistance for the active solid phase in order to account for the resistance degradation of particle-particle contacts caused by internal stresses. The detailed mathematics and diagram of TML are beyond the scope of this note and are shown elsewhere (98).

A three electrode system was used for EIS measurements, consisting of a platinum counter electrode and Hg/HgO reference electrode. An 8 mole kg^{-1} KOH electrolyte solution with 1 % LiOH was used in all the experiments. The working electrodes were planar nickel, rolled and bonded porous nickel, and sintered, porous nickel.

EIS was measured using a Solartron 1250 frequency response analyzer coupled with a potentiostat. An equivalent circuit for planar nickel electrode was suggested (98):
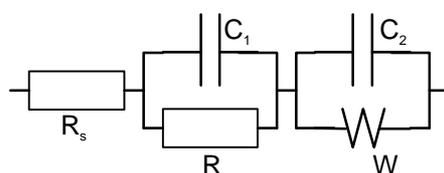
For porous rolled and bonded electrodes, a total of 16 independent variables were used to describe the impedance of porous nickel battery electrodes. The TML was used to model the degradation processes. Each of the 16 variables in the model was first determined as accurately as possible in separate experiments. Impedance spectra were then calculated from the model and were compared with porous nickel electrode impedance spectra. The experimental and calculated impedance spectra are plotted in Fig. 16.
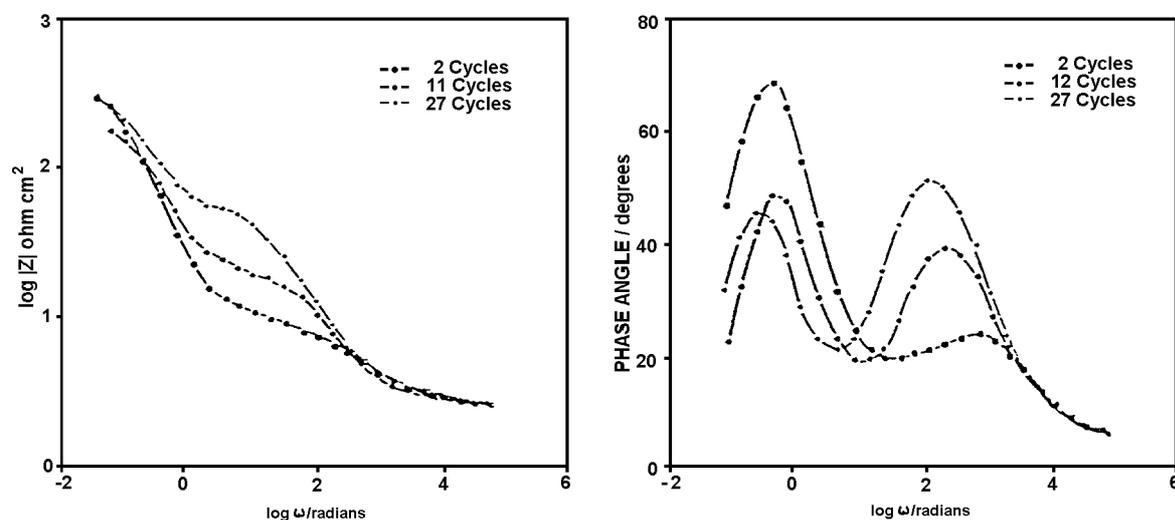

**Fig. 16 Bode plots for a rolled and bonded porous electrode
at 0 mV and 23°C after various cycles (98)**

7. Ni-H$_2$ Cells in KOH Solutions

The impedance of Ni electrodes has been measured by many investigators. The effect of electrolyte concentration on the life of Ni-H$_2$ cells has been studied recently (100-112), and EIS has been used to study the Ni-H$_2$ cells in various concentrations of KOH solution (101). In this latter study, impedance was measured for a number of electrodes that had been cycled in concentrations from 21% to 36% KOH at 80% depth of discharge (DOD) condition to failure. Cell life ranged from about 1000 to 40000 cycles. The impedance spectra were obtained for the uncycled electrode and the failed electrodes after 1000 to 40000 cycles.

EIS measurements were carried out using Solartron 1250 frequency response analyzer and a Solartron 1286 potentiostat; data were taken using ZPLOT software (4,5) over frequencies of 1000 Hz to 1 mHz. At high frequencies ac signal was 1 mV rms and at low frequencies ac signal was 5 mV rms. A Hg/HgO reference electrode was used in the experiments. In order to bring the failed electrodes as much as possible to a consistent state, they were cycled ten times, starting with four cycles at a C/10 charge rate for 18 h and a C/4 discharge rate to a cut-off voltage of -0.50 V. The next five cycles were at a C/4 charge rate with 10% overcharge and a C/2 discharge rate to 80% DOD. They were then charged again at a C/4 rate with 10% overcharge before taking the impedance measurements, starting with the highest voltages. Before the measurements, the electrodes were equilibrated at the desired voltage, usually until the dc current fell below 10 mA. The electrode that had not been used in the cycling tests was conditioned in the same way.

The impedance data were simulated using both EQUIVCRT and CNLS programs. The first proposed interface model is shown as:
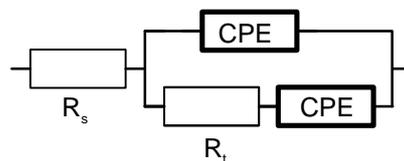
The experimental and simulated impedance spectra using EQUIVCRT is plotted in Fig. 17.
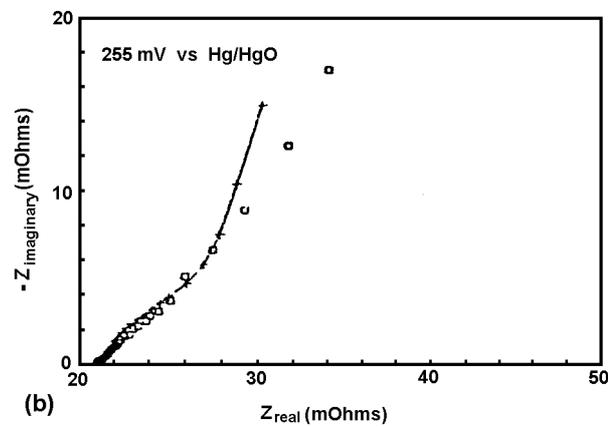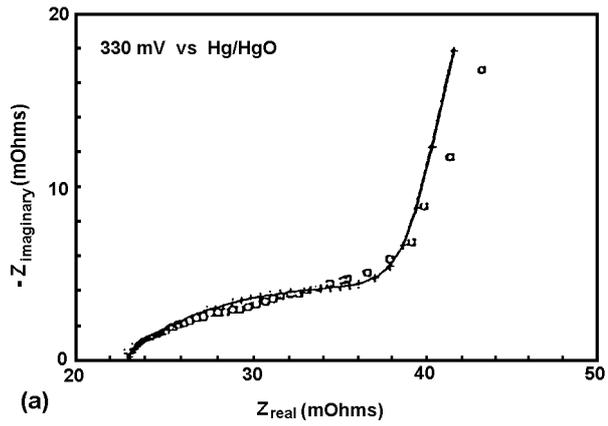
Fig. 17 The experimental and fitted impedance spectra using Equivalent Circuit software (98)

The second proposed interface model is expressed as follows:
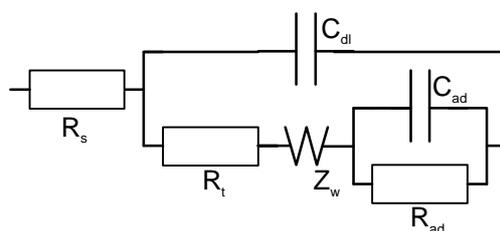
The experimental data were simulated using the LEVM-CNLS program and plotted in Fig. 18. This provided the better fit and indicated that the second proposed interface model was reasonable. Impedance parameters using the second interface model for the uncycled electrode are shown in Table 2 below; the voltage is versus Hg/HgO reference electrode.

TABLE 2 : Impedance Parameters for Ni uncycled electrode

Parameter	0.330 V	0.290 V	0.255 V	0.200 V	0.170 V
R_t (Ω)	0.0052	0.0007	0.057	0.048	0.118
C_{dl} (F)	1.19	3.65	0.48	0.43	0.50
R_{ad} (Ω)	0.0066	0.0009	0.0078	0.011	0.0097
C_{ad} (F)	41	75	123	3.7	350
R_{diff} (Ω)	0.17	0.15	0.56	0.59	1.00
T	479	436	420	443	477
Phi	0.70	0.67	0.65	0.63	0.61

R_{diff} is the kinetic resistance, and T and Phi are related to the contribution of the diffusion element.

Unfortunately, the experimental impedance data after 1000 to 40000 cycles were not analyzed, and so there was no comparison between uncycled and failed electrodes
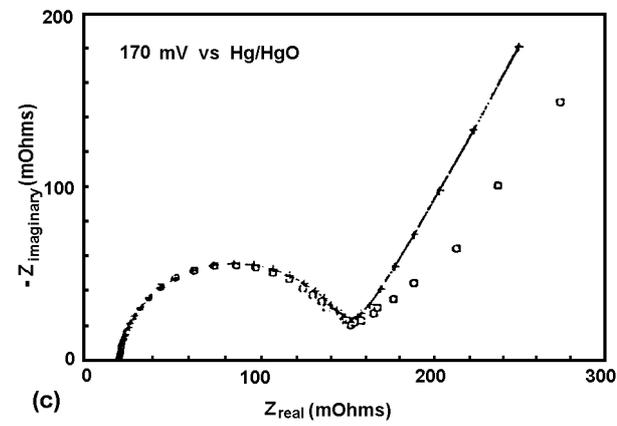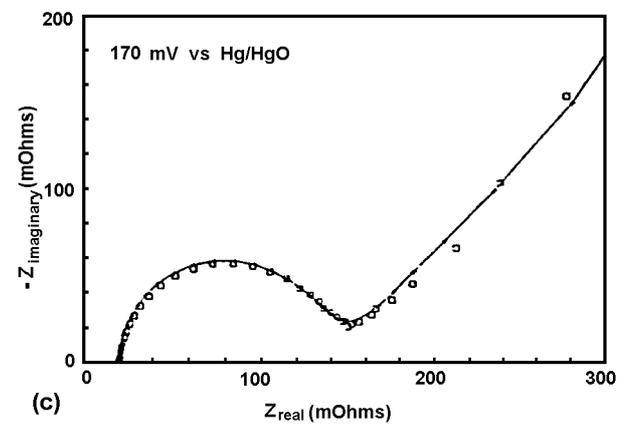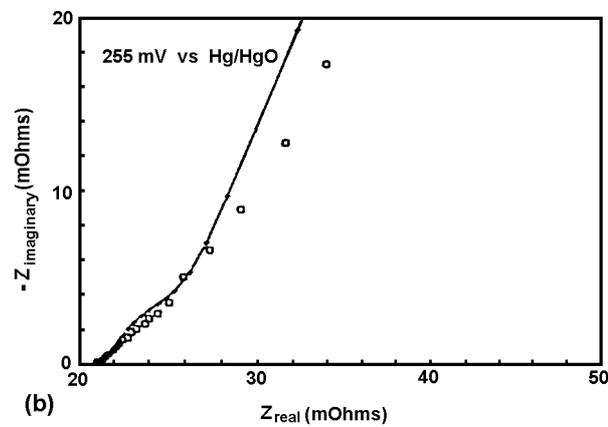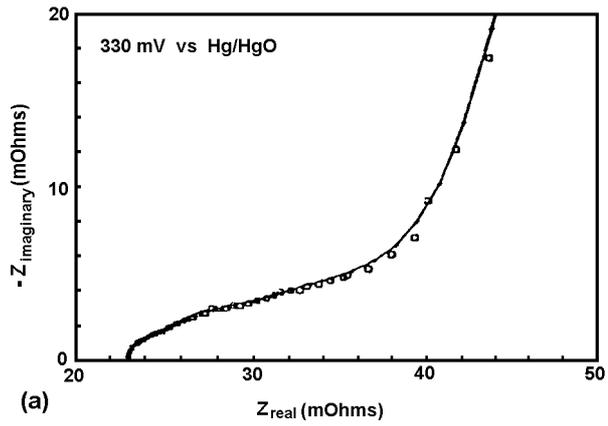
Fig. 18 The experimental and fitted impedance spectra using ZFIT-CNLS software (98)

using impedance data. The Ni electrode after over 30000 cycles showed a small kinetic resistance, R_t and a small Warburg impedance in 26% KOH solution, but a complete data analysis using the second interface model would be necessary for the cycled Ni electrode in order to build up the correlation between impedance data and life and performance of the electrodes.

8.   Ni/Ni(OH)$_2$, Ni/Cd(OH)$_2$ and Ni/H$_2$ Cells

Armstrong and Charles (113) have applied EIS in the study of Ni-Cd cell across the nickel/cobalt hydroxide range in alkaline solution. The impedance measurements were carried out using a frequency response analyzer coupled with a potentiostat. Hg/HgO was used as the reference electrode. From the experimental results, a relationship between electrode surface area and electrode capacity was identified, which was complicated by the presence of cobalt due to increased film conductivity and by changes in the amount of active materials deposited. The addition of cobalt to the system improved the electrode kinetics by lowering the charge-transfer resistance of the reaction process. The typical Nyquist plots are shown in Fig. 19.
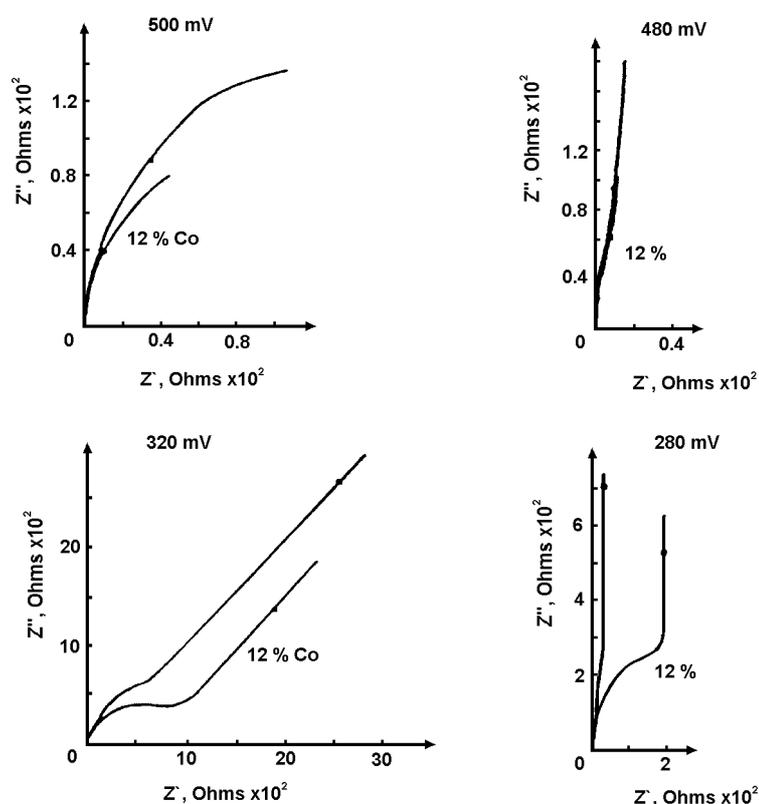
Fig. 19 Typical impedance spectra for 0% and 12% cobalt thin film electrodes at 500 mV, oxygen evolution; 480 mV, charged; 300 mV redox reaction; and 280 mV, discharged (113)

Reid (114) has applied EIS in the study of Ni/Cd and Ni/H$_2$ flightweight cells using the case as a reference electrode. A Solartron 1250/1286 combination was used for EIS measurements on two flightweight 50 A h Ni/Cd cells from Gates which had been stored for six years before the measurements, and one flightweight 50 A h Ni/H$_2$ cell from Hughes which had performed 900 real-time cycles followed by three years on open-circuit, charged to 1.275 V and equilibrated overnight.

The impedance spectra showed a one time-constant model with Warburg impedance at the low frequencies shown below:
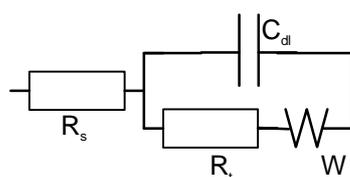
The experimental results show that the cell case can be used as the reference for Ni/Cd cells, and may be also be used as a reference for Ni/H$_2$. The EIS measurements can be used to determine which electrode is responsible for the loss of performance.

9.   Metal Hydride Electrodes

The nickel metal hydride (Ni/MH$_x$) battery developed in recent years is one of the most promising secondary batteries because of its high energy density, high rate capability, and environmental acceptability. The nickel metal hydride electrode is the negative electrode in the battery with hydrogen being stored in the alloy. The electrode reactions at the negative and positive electrodes can be expressed as follows (115):

$$M + H_2O = MH + OH^-$$

$$Ni(OH_2) + OH^- = NiOOH + H_2O + e^-$$
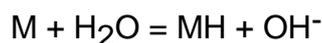
The mathematical model of Viitanen (116) predicts the polarization behaviour of a metal hydride electrode, considering both charge transfer and mass transport processes. In this model, the charge transfer reaction at the surface of alloys, the

diffusion of hydrogen in metal, the ionic transport in the electrolyte and electronic transport in the solid phase are considered as the intermediate steps of the hydriding/dehydriding reaction, and the charge transfer reaction at the surface is the rate-determining step.

Only a few previous EIS studies on $NiMH_x$ have been reported. Kuriyama et al (117,118) applied EIS to study the degradation mechanism of metal hydride electrodes and the activity of the alloy. They found that the kinetics of the electrochemical hydriding/dehydriding reaction of an alloy electrode depended upon the reaction resistance at the alloy surface. Agarwal et al (119) applied mathematical analysis to elucidate the results of EIS. Zhang et al (115) also developed a mathematical model to study the mechanism of the hydriding/dehydriding reactions and the effect of structure and composition of $NiMH_x$ electrodes in order to enhance the performance of the metal hydride electrodes for battery use.

The simplified interfacial model of an ingot $NiMH_x$ electrode, without considering diffusion processes (115), is shown by
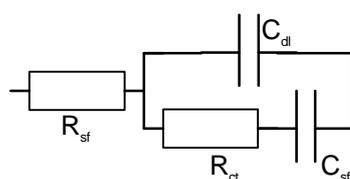
where R_{sf} and C_{sf} are the pseudo-capacitance of the surface reaction and the ohmic resistance of the electrode respectively.

EIS results for planar electrodes were recorded on an ingot of the hydriding alloy at a potential of -0.7 V vs. Hg/HgO reference electrode. The impedance spectra, shown in Fig. 20, followed the model proposed (115) and the mechanism of the electrode hydriding/dehydriding reaction was a charge-transfer control process. The impedance is very high (of the order of 1 MΩ at 0.001 Hz), and the high-frequency impedance cannot be seen clearly in the Nyquist plot. It should be noted that Bode plots could be more useful in this situation since there may be a time constant in the high frequency region which cannot be observed from the Nyquist plot.

EIS experiments were also performed on porous electrodes (Fig. 21), and a three-time constant model was proposed (115). Again, Bode plots may provide more detail of impedance spectra at high frequencies because only two time constants can actually be observed from the Nyquist plot. The impedance was much lower than that of the planar electrode (1.4Ω at 0.001 Hz).
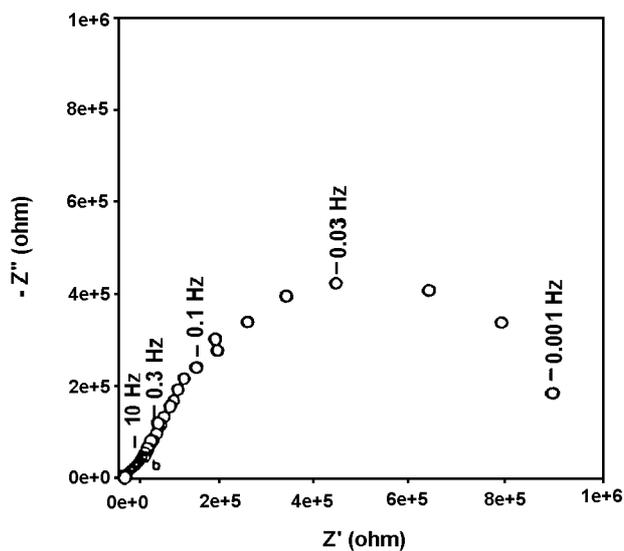
Fig. 20 Nyquist plot for LaNi$_{3.55}$Mn$_{0.4}$Al$_{0.3}$Co$_{0.75}$ ingot sample, surface area 2mm^2 (115)
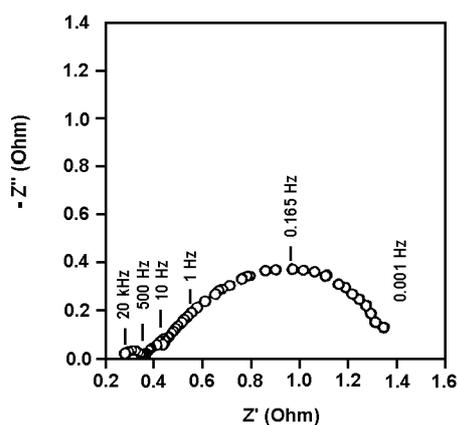
(a)
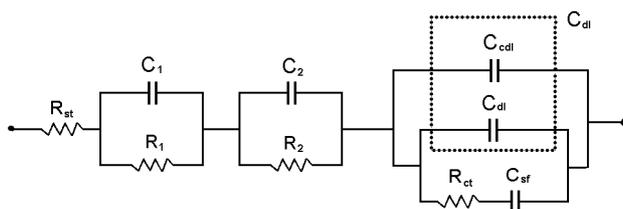
Fig. 21 Typical Nyquist plot of MH$_x$ electrode and proposed equivalent circuit (115)

10. Lithium in SO$_2$ Electrolytes

Although EIS has been predominantly applied in the study of practical Li/SO$_2$ cells (120-124), the passivation of lithium in SO$_2$ was not studied in detail. In order to understand this process, the passivation of lithium in SO$_2$ electrolyte solutions has been investigated by Geronov et al (120). EIS offers a convenient means for studying the kinetics of lithium passivation, and the impact of the carbon cathode on the impedance parameters, especially in a wider frequency range, cannot be neglected.

EIS measurements were carried out by a Solartron transfer function analyzer connected to a computer in the frequency range from 10^5 to 0.1 Hz. The surface area of the electrode was 0.125 cm². The interface model of the experimental data showed a one-time constant model with solution resistance in series with a parallel network C$_g$ and R$_f$, where C$_g$ is the geometric capacitance and R$_f$ is the film resistance on lithium shown below:
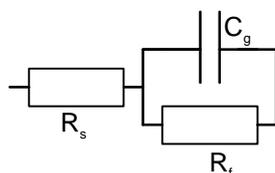
At 55°C in an electrolyte containing 33% SO$_2$, the film resistance of lithium electrode increased with the storage time. Values of R$_f$ were about 140, 220, 415, and 500 ohms after 0.5 h, 2 h, 64 h, and 110 h respectively. At 22°C, for a lithium electrode kept for 2 h in a dry room at 3.2% relative humidity (RH) and then stored at room temperature in an electrolyte solution containing 35% SO$_2$, film resistance decreased with storage time. The values of R$_f$ were about 16000, 6500, and 450 ohms after 10 min, 5 h, and 20 h storage, respectively. The surface film was dissolved by SO$_2$ and the usual dithionate film with a lower resistance was formed. Since the charge transfer resistance (R$_t$) on clear Li surfaces was about 3-5 ohm.cm², much less than the value of R$_f$, the effect of R$_t$ can be neglected.

It is obvious that lithium electrodes form a good passivating film in an electrolyte containing SO$_2$ at 55°C, but not at 22°C.

11. Li/SOCl$_2$ and Li/SO$_2$Cl$_2$ Cells

The Li/SO$_2$Cl$_2$ cell has a higher open circuit voltage than the Li/SOCl$_2$ cell (3.9 V vs. 3.7 V) and may have a higher energy density in a fully engineered cell. From the accepted discharge reactions, Li/SO$_2$Cl$_2$ is also possibly safer than Li/SOCl$_2$,

$$4Li + 2SOCl_2 = 4LiCl + S + SO_2$$

$$4Li + 2SO_2Cl_2 = 4LiCl + 2SO_2$$
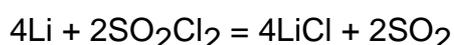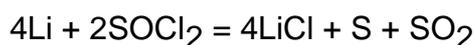
Sulfur is formed only in the case of Li/SOCl$_2$, and has been identified by DTA study (123) as a potential reactant with lithium in a thermal runaway condition. But the main problem in the development of the Li/SO$_2$Cl$_2$ is the corrosion of lithium in sulfuryl chloride electrolytes. Evolution of gas from lithium immersed in SO$_2$Cl$_2$ - LiAlCl$_4$ solution has been observed (124).

EIS has been used to study the formation and disruption of the film in a Li/SO$_2$Cl$_2$ cell. The impedance spectra showed the film resistance increased with immersion time in the electrolyte. A Randles circuit model was observed as shown below:
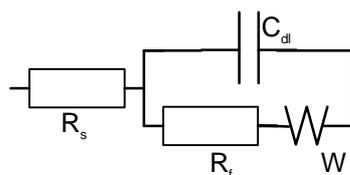
R$_f$ increased from 28 ohm after 4 h immersion to 31 ohm (6 h), and 120 ohm later. The thickness of the surface film increased with immersion time and reached 1410 Å after 17 days storage. From the impedance data, the thickness of the surface LiCl film changed under polarization condition. At 0.1 V polarization, the resistance of the LiCl film was 58 ohm. It decreased further to 39 and 31.5 ohm at polarizations of 0.2 V and 0.3 V, respectively, but built up again after termination of polarization. The recovery of film thickness following polarization was tracked by measuring the change of impedance.

The behavior of the passivating film on lithium in sulfuryl chloride has been studied by EIS. The thickness of the passivating film increased with the storage time and the film was disrupted by the passage of current.

EIS has also been applied to the study of the anodic passivating layer in $Li/SOCl_2$ batteries (125-133). The postulated overall cell reactions in a neutral $Li/SOCl_2$ system have been summaried by Madou et al (130). The highest cell voltage at 3.72 V corresponds to the following reaction:

$$4Li + 2SOCl_2 \rightarrow 4LiCl + S + SO_2$$
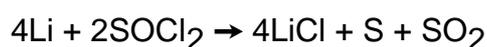
and the lowest cell voltage at 3.52 V corresponds to the reaction:

$$8Li + 4SOCl_2 \rightarrow 6LiCl + S_2Cl_2 + Li_2S_2O_4$$

The impedance spectra showed a one time-constant model for the $Li/SOCl_2$ system. The resistance of the passivating film after filling with the electrolyte increased with time. The passivating LiCl film became more resistant with the increase of immersion time in electrolyte (125). After an anodic pulse, the passivating layer on the Li electrode was disrupted and the resistance of the passive film decreased dramatically. But the passivating film would build up again in time after the anodic pulse. The interface model can be described as follows:
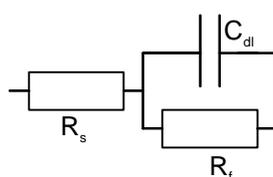
The time relation of impedance is shown elsewhere (125,126).

EIS is very sensitive technique for following the changes of the passivating film on Li electrodes in $Li/SOCl_2$ batteries and for characterising the property of the surface film.

12.   EIS Studies of Na/S Cells

The high power and energy densities of the sodium-sulfur battery have led to it being considered for a wide variety of applications, for example, utility load levelling,

automotive traction and satellites. The basic reaction in the Na/S battery was described by Halpert (1) as follows:

Na/Beta Alumina/S

The theoretical specific energy is 790 Wh/kg and the open circuit voltage is 2.08 V. Na/S cells show high specific energy. Since the operating temperature is about 350°C and operating voltage is 1.7 V, the issues for Na/S batteries are thermal control, low volumetric energy density, and materials problems including corrosion. Ceramic electrolytes and separators are also important considerations for this type of battery.

Previous studies of cell impedance have primarily concentrated on elucidating the mechanisms of cell operation, and diagnosing the cause of poor cell performance (135-136). The impedance measurements were concentrated on higher frequencies. McKubre et al (134) have extended these measurements into the milliHertz region, which are quite necessary for measuring a battery in service.

Johnson has applied impedance to follow Na/S cells as a function of state of charge at very low frequencies such as 10^{-5} Hz (135,136). A Solartron 1250 Frequency Response Analyzer and 1286 potentiostat were used. The frequencies were swept from 100 Hz to 5×10^{-5} Hz. The cells were progressively discharged in one ampere-hour steps, and an equilibration period of at least one hour was allowed prior to each measurement.
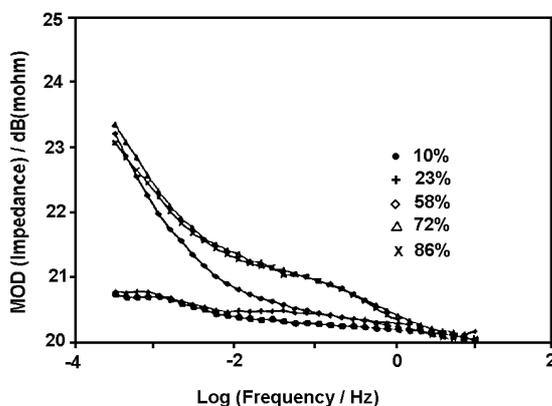
a.   b.
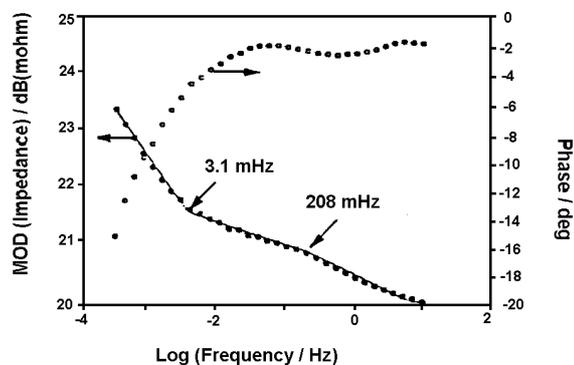
Fig. 22 Bode plots for a Na/S cell (136)
a. at five different states of discharge   b. at 72% discharge

The Bode impedance plot for the cell at five different depths of discharge are shown in Fig. 22a (136). Impedance increased greatly at low frequencies (below 10 mHz) when the cell operated in the single-phase region (i.e. at depths of discharge greated than 56%). This phenomenon is shown more clearly in Fig. 22b for the cell at 72% discharge level. The so-called "corner" frequencies of 3.1 mHz and 208 mHz correspond to relaxation times of 321 seconds and 4.8 seconds respectively. At low discharge states, such as 10% and 23%, the impedance shows a low charge-transfer resistance without any mass transport effect. At high discharge states, such as 58%, 72% and 86%, the impedance spectra show an increasing charge-transfer resistance and a Warburg impedance which indicates the effect of mass transport. The dispersion evident at very low frequencies in the single-phase region shown in Figs. 22a and 22b is most likely the response characteristic of the sulfur electrode, as this was the only electrode which changed composition with depth of discharge.
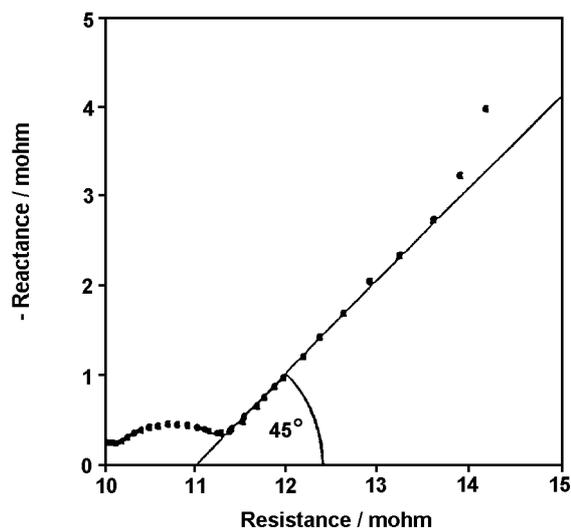
Fig. 23 Nyquist plot for a Na/S cell at 72% discharge (136)

The Nyquist plot at 72% discharge (Fig. 23) provides strong support to the hypothesis that discharge polarization arises due to concentration gradient across the high resistance barrier layer; details of the analysis were discussed by McKubre (134) and Johnson (136). The interface model was described (136,137) as:
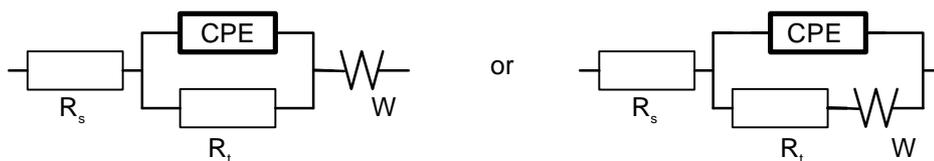
The details of data analysis for a simple one time-constant model have been described by Macdonald and Johnson (137). The Nyquist plot for the cell at 95% discharge displayed three different regions: a high frequency depressed semi-circle which provided C_{dl} and R_t, and a Warburg impedance region; below 0.4 mHz, the capacitive component of the cell impedance increased greatly which indicated the existence of concentration polarization in Na/S cells.

13.   Separators in Rechargeable Lithium Batteries

Separators can be used as internal safety devices by closing down the pores during short-circuit abuse (138-140). It has been demonstrated that for Li/V$_2$O$_5$ rechargeable AA size cells, by choosing the appropriate combination of separators, the cell can be made safe to high rate overcharge as well as short-circuit abuse (141).

EIS has not only been applied to the study of batteries, but has also been used to evaluate separators in rechargeable lithium batteries. The importance of this study is obvious. The melting of separators which causes the decrease of separator pores results in a large reduction in current flow. Measurement over a range of temperature can provide the melting temperature, rate of a pore fusion, and dimensional stability temperature. A good separator, with respect to improved safety of a lithium cell, should have the following properties: the melting point should be high enough not to interfere with normal use of the battery, while the dimensional stability temperature and the rate of shutdown should be high.

Laman et al have carried out these measurements using a specific frequency (1kHz) in their ac impedance measurements (141). Four separators and their combinations were measured at different temperature. The results are shown in Figs. 24 and 25.
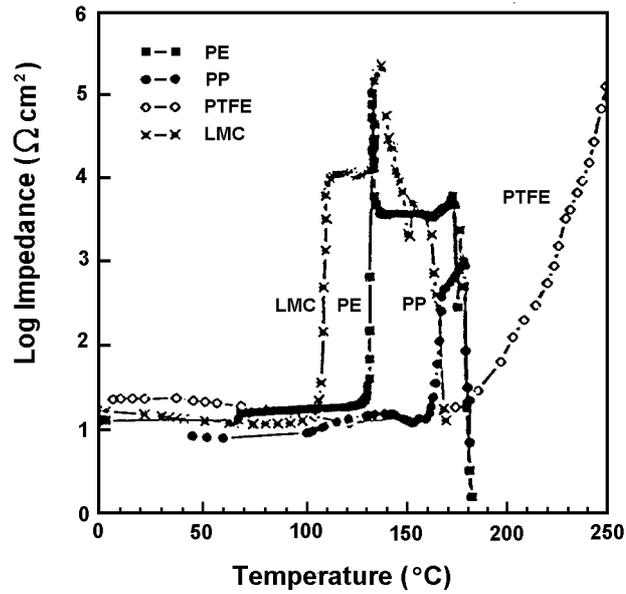
Fig. 24 The ac impedance data at 1 kHz for electrolyte filled microporous polyethylene (PE), polypropylene (PP), polytetrafluoroethylene (PTFE), and low melting point composite (LMC) separators, as a function of temperature (141)
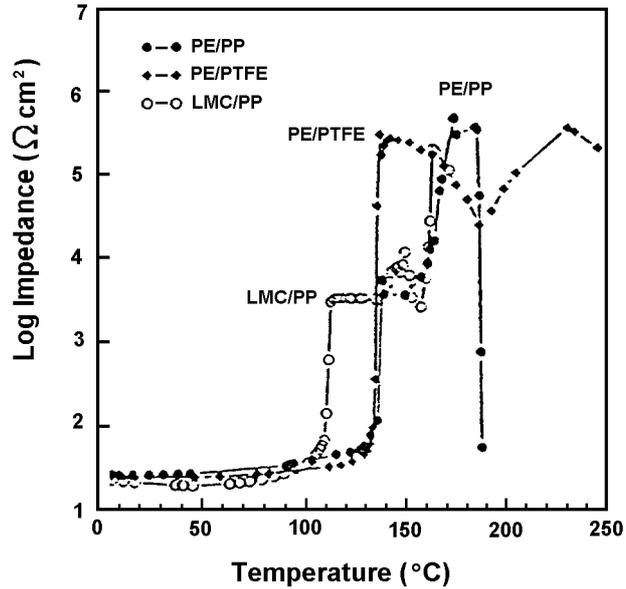
Fig. 25 The ac impedance data at 1 kHz for combinations of electrolyte filled separator presented in Fig. 24 (141)

Fig. 24 shows the change of impedance as a function of temperature for four different separator sheets. Melting points are 118°C, 151°C, 324°C, and 88°C for polyethylene (PE), polypropylene (PP), polytetrafluoroethylene (PTFE), and low melting composites (LMC), respectively. The results show that when the cell is heated to a few degrees above the meilting point of the separator, pore closure causes the electrical impedance to rise rapidly by several orders of magnitude. Assuming an initial impedance of 200 milliohm for an AA size cell and a compliance voltage for the charger of 10 V, an increase in cell impedance by three orders of magnitude will reduce the maximum allowable current during overcharge abuse to a safe value of 50 mA. Fig. 25 shows the electric impedance data of the combined separators with temperature. It is obvious that using separator combinations is an effective way of achieving a wide insulating range.

14.   Conductive Polymers

With the development of solid-state batteries, there is a need to characterize electroactive polymers, and EIS has been applied in this research. Musiani (142) has reviewed EIS application on either redox or conducting polymer layers. Electroactive polymers in thin film form have now become an actively investigated subject (142-146). Fig. 26 shows a $Li/PEO/V_6O_{13}$ battery configuration (147).
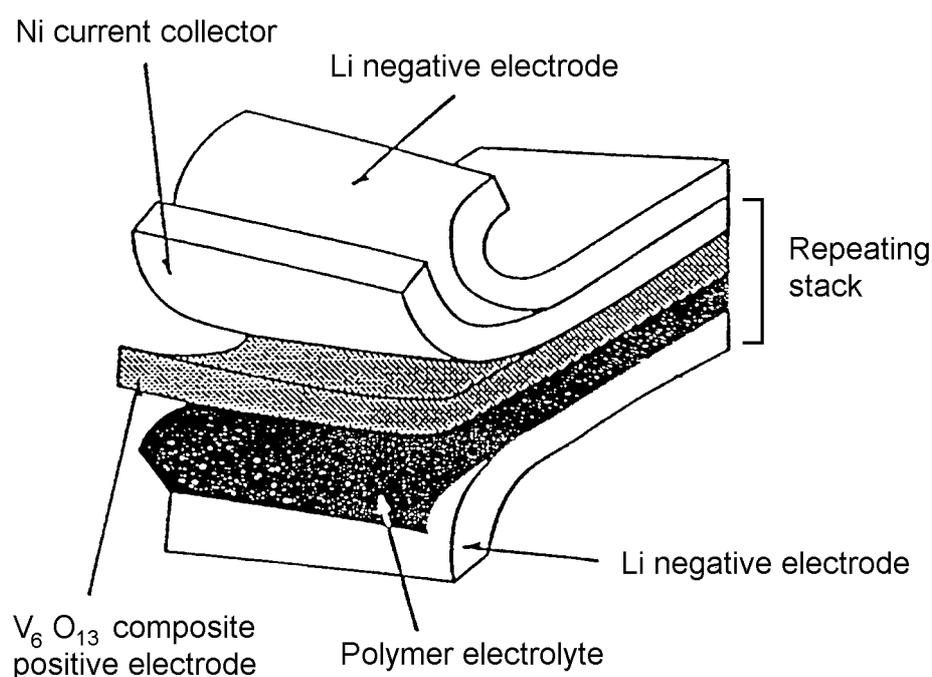
Fig. 26 The configuration of a $Li/PEO/V_6O_{13}$ battery (147)

The battery contains a Li negative electrode, Ni current collector, polymer electrolyte, and V_6O_{13} composite positive electrode. In comparison with NiCd and lead-acid batteries(2), it is obvious that the lithium polymer battery has high energy density, power density, high cell voltage, wide operating temperature, low self discharge rate (0.1 % / month), great flexibility, excellent safe storage and operation, but at present only a limited number of charge cycles.

14.1 Redox polymers

A kinetic model for an electrode coated with a redox polymer layer in contact with a solution containing no redox couple has been proposed by Gabrielli et al (148). Electron transfer at the metal-polymer interface occurs following the Bulter-Volmer equation. The faradaic impedance is calculated and shown below:

$$Z_F(\omega)=R_t(1+((k_f+k_b)/(j\omega D_E)^{\frac{1}{2}})coth\Phi(j\omega/D_E)^{\frac{1}{2}})$$

where R_t is the charge transfer resistances and D_E is the diffusion coefficient of electrons.

The typical ac impedance diagram is predicted by Gabrielli et al (148). The impedance corresponds to a Warburg impedance at high frequency and a series resistance (R_p) and capacity (C_{LF}) circuit at low frequency. An experimental investigation was carried out on Ru(bpy)$_2$Cl(PVP)Cl deposited on vitreous carbon in 1 M HCl (167). The results were found to be in good agreement with Gabrielli's model. Another experiment investigated redox polymers in poly(vinylferrocene) deposited on Pt in 0.1 M TBAP-CH$_3$CN (149). The results was discussed by C. Ho et al (150).

One possible application of a polymer modified electrode is electrocatalysis. The overall rate of the mediated electrochemical process depends on the following processes:

- Charge transport across the film
- Exchange reaction
- Molecular diffusion of substrate in the polymer
- Convective diffusion of substrate in solution

The impedance model for a redox polymer film in contact with a solution containing a redox couple has been calculated (148,151,152)

14.2   Conducting polymers

Polyphenlene (153), polythiophene (154), poly-3-methylthiophene (155), polythienothiophene, polydithienothiophene (156), and poly-N-ethylcarbazole (157) have been studied by ac impedance. The detailed information is described in the above literatures. Bruce et al (158) have studied the electrode/electrolyte interfaces in cells of the type $Li/PEO-LiCF_3SO_3/V_6O_{13}$ by EIS. At 100°C, for the V_6O_{13}/solid electrolyte interface, EIS showed a two time-constant model. In the high frequency semicircle, R_{st} increased and C_{st} decreased with time by a factor of five during a 200 h time period. The interface model was not clear in this paper. It is believed that the high frequency semicircle corresponds to a charge transfer process and the low frequency semicircle demonstrates a finite mass transfer process (Warburg impedance and CPE). For the V_6O_{13}/liquid electrolyte (methoxy end-capped short chain PEO) interface, the impedance also showed a two time-constant model with CPE contribution at the lowest frequencies. At the lithium/solid electrolyte interface, the impedance showed a one time-constant model and R_{ct} increased with time after the assembly of the cell. This results are similar to that obtained by Fauteux (159). At the lithium/liquid electrolyte interface, the impedance showed two well defined semicircles at all times.

15.   EIS Studies of Fuel Cells

Impedance measurements have been widely used in the study of fuel cells; Selman and Lin (3) have summaried this application, focussing on the electrode/electrolyte interface. The in-situ characterization of experimental fuel cells using EIS was also studied and summaried by Jenseit et al (160). The combinations of current-voltage curves and impedance spectroscopy data of fuel cell electrodes provided the information to understand the influence of electrode morphology on effective electrocatalytic behavior of electrodes for alkaline and molten carbonate fuel cells. PTFE-bonded Pt-activated carbon electrodes, PTFE-bonded Raney-nickel anodes, Ni-sponge anodes, and NiO-cathodes were discussed. The limitations of EIS on fuel cell study were mainly due to the explanation of EIS data and very fast electrode kinetics (3).

There are five main types of fuel cell (161): the alkaline fuel cell (AFC), the polymer electrolyte membrane fuel cell (PEMFC), the phosphoric acid fuel cell (PAFC), the molten carbonate fuel cell (MCFC) and the solid oxide fuel cell (SOFC). Schematics of these fuel cells are shown in Fig. 27. The cathode and anode of a fuel cell are both porous in order to increase the reaction area and thereby the total current generated. Fuel cell technology has been extensively described in recent monographs (162,163).
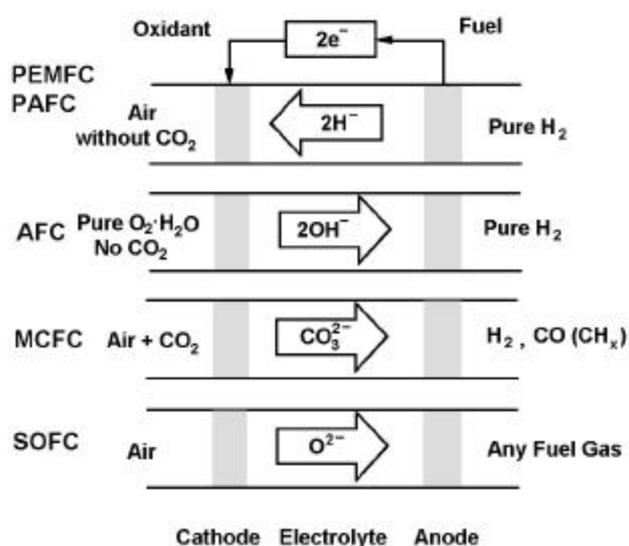
Fig. 27 Schematics of five main types of fuel cells (161)

EIS was first applied to porous electrodes by De Levie (164), and the modeling of porous electrodes has been discussed by Raistrick (165). As an in situ technique, EIS is very attractive in fuel cell applications. The following sections provide an overview of the application.

15.1   Ionic Conductivity of SOFC and PEMFC

EIS was used as a tool to determine the ionic conductivity of SOFC and PEMFC in the early stages, and this application is still predominant. A particular equivalent circuit has been used very often and is shown below (166):
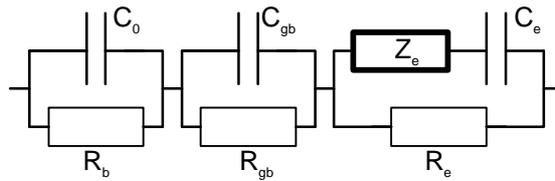
where R_b is the bulk resistance, C_o the corresponding capacitance, R_{gb} and C_{gb} are the resistance and capacitance of the grain boundary, R_e is the kinetic resistance and C_e the capacitance of the electrode, and Z_e is the mass transfer contribution.

The ac characteristics of the PEMFC have been studied recently. The dynamic ac impedance studies were reported by Parthasarathy et al (167); the equivalent circuit was similar to that of SOFC. Springer et al have studied polymer electrolyte fuel cells using ac impedance spectroscopy (168) to characterize the performance of fuel cells.

15.2   Electrode Reaction Mechanisms

Verkerk et al developed a model to describe the oxygen reduction at a porous platinum electrode in contact with a solid ionic conductive electrolyte (169). The interface model is shown below. Oxygen is supplied by diffusion and adsorption to the electrode reaction zone, W is the Warburg impedance and R_{ct} is the charge transfer resistance, and R_b is the contact resistance.
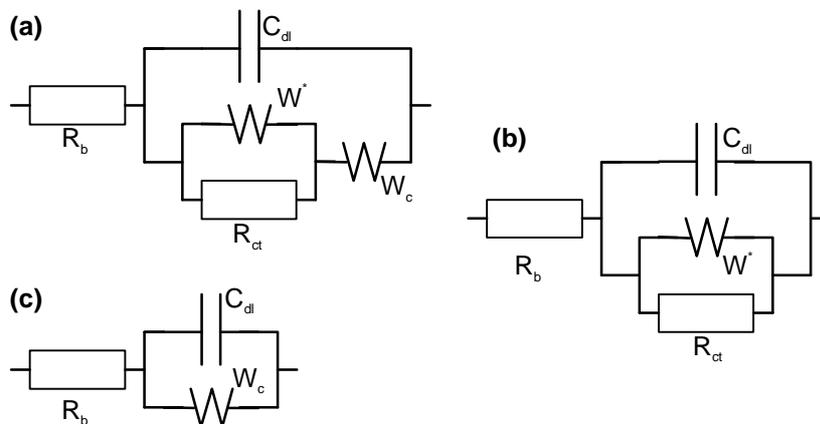
For MCFC, EIS is mainly used in the study of reaction kinetics of the cathode and the reaction order of oxygen and CO_2 (170,171). In order to determine the reaction

mechanism, EIS data analysis based on equivalent circuits has to be used. The interface parameters can be obtained by this analysis, but it is important that the parameters should have clear physical meaning. Nishina et al (172,173) used the following interface model to fit EIS data of MCFC electrode reactions at Au and NiO-coated flag electrodes.
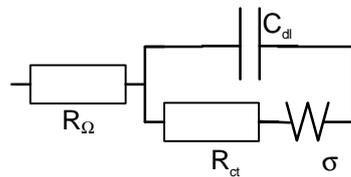
They found that the superoxide reaction path was dominant in the reduction of oxygen in Li_2CO_3-K_2CO_3 eutectic melts, while the simultaneous diffusion of O_2^- and CO_2 limited the reaction-related mass transfer. Lee and Selman (174) and Makkus (175) have also studied the reaction mechanism of other MCFC systems.
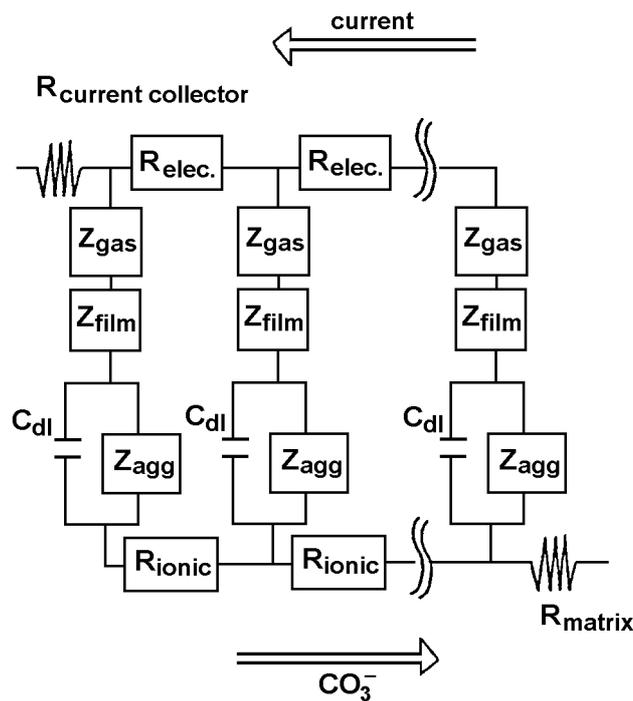
**Fig. 28 Distributed parameter network equivalent circuit
of a gas-diffusion porous electrode (178)**

In a fuel cell, distributed-parameter effects determine the performance. This is due to the non-uniform potential distribution which causes a non-uniform electrode impedance along the pores. These effects are the main limitation in using EIS to study the porous electrode reactions in a fuel cell, as demonstrated by the complicated distributed-network model shown in Fig. 28 (176-178).

15.3   Study of Gas Diffusion Electrode

Materials development and technology are the major tasks in designing a fuel cell. EIS has been successfully applied for in-situ characterization of the gas diffusion electrodes (160).   Fig. 29 shows the typical structure for a PTFE-bonded gas diffusion electrode made from Pt-activated soot particles containing nanopores, which form agglomerates of submicrometer to micrometer size. This type of electrode is used for phosphoric acid fuel cells, and alkaline fuel cells (179-181). The morphology of PTFE-bonded Raney-nickel anodes used in alkaline fuel cells is shown in Fig. 30 (174,182).
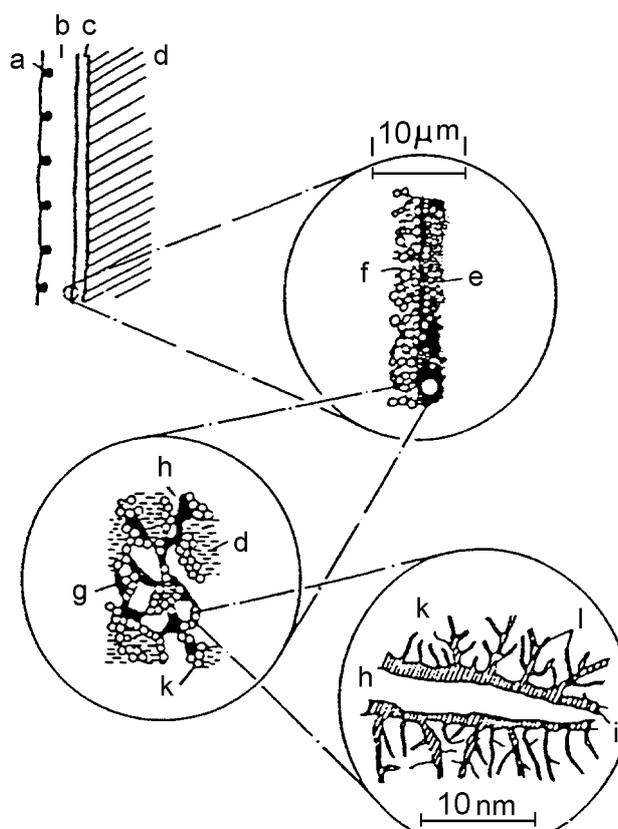
Fig. 29 Structure of PTFE-bonded soot electrodes (160)
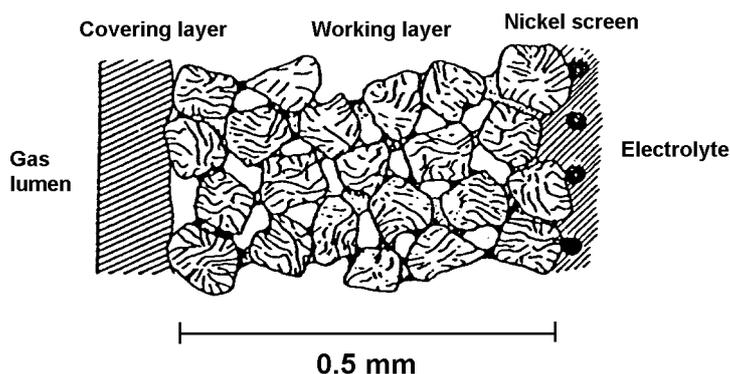
Fig. 30 Morphology of PTFE-bonded Raney-nickel anodes (160)

The experimental preparation and procedures are shown elsewhere (174). Morphological data of different gas diffusion electrodes are listed in Table 3.

Table 3 - Morphological data of different gas diffusion electrodes

Morphological data	Silflon	Vulcan XC(10%Pt) Raney-Ni	Vulcan XC 30% PTFE	30% PTFE
Catalyst loading ($mgcm^{-2}$)	$17(1.7)^*$	11	120	90
Thickness of electrode (mm)	0.45	0.25	0.6	0.6
Specific catalyst surface (m^2cm^{-2})	4.7(0.17)	1.04	0.24	5.7
Electronic conductivity of electrode matrix$^+$($\Omega^{-1}cm^{-1}$)	2.5	1.34	∞	1.8
Specific electrode resistance (Ωcm^2)	0.018	0.018	0.0	0.033

* The contribution of platinum is in parentheses.
+ Conductivity of electrode materials with metal-gauze support.

Fig. 31 shows the model used to interpret the electrochemical impedance spectroscopy according to Raistrick (176). R_1 is the charge transfer resistance, R_{dia} is the diaphragm resistance, R_2 and C_2 describe the mass transfer impedance in
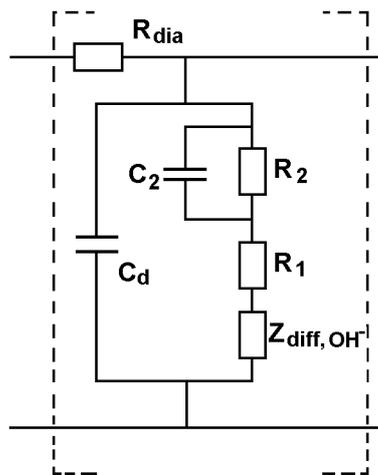
Fig. 31 Impedance model used for interpreting impedance spectroscopic data (160,176)
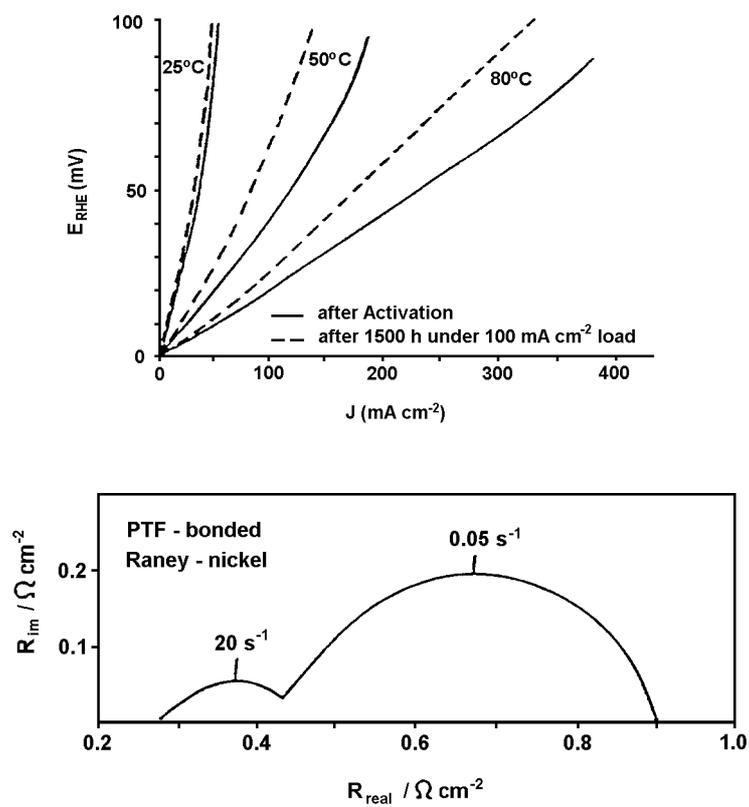
Fig. 32 Current-voltage curves and impedance spectra of Raney-nickel anodes (160)

the microporous electrolyte matrix, C_d is the double layer capacitance, Z_{dif} is the mass transfer impedance of fuel and hydrogen across a thin electrolyte film, and the combination of R_1, R_2, and C_2 comprise the electrochemical Thiele modulus and catalyst utilization. The partial catalyst utilization is characterized by electrochemical Thiele modulus Φ.

For Raney-nickel anodes, the Nyquist plot of the electrode is shown in Fig. 32. The measurement was carried out at near-equilibrium potential. The Nyquist plot shows a small semicircle with 45° slope at the high frequency end due to the diaphragm resistance, followed by a flat, distorted semicircle at the low frequencies. The high frequency 45° phase angle may correspond to a mass transfer process which was modeled and discussed by Lorenz and Mansfeld (183,184). The potential and current relations at three different temperatures are also shown in Fig. 32; the performance improves remarkably with temperature. According to the impedance data, this is due to the decrease of diaphragm resistance and a decrease of charge transfer resistance at high temperature. The interface parameters of the Raney-nickel electrode are listed in Table 4.

Table 4 - Interface parameters of the Raney-nickel anode

Temperature (°C)	25	25	25	50	80
Current density (A/cm²)	20	82	143	5	5
Overpotential (mV)	30	100	150	2.0	0.5
R_{dia} (Ωcm²)	0.53	0.55	0.45	0.36	0.19
C_d (F/cm²)	1.0	1.1	1.2	1.1	1.0
R_1 (Ωcm²)	25	20	28	10	4
R_2 (Ωcm²)	0.23	0.32	0.75	0.12	0.09
C_2 (F/cm²)	10.5	12	14	11	12
R_{diff} (Ωcm²)	0.04	0.06	0.05	-	0.035
Thiele modulus Φ	9	16	27	11.5	22.5

By increasing the load at the same temperature, R_{dia} and C_d are almost constant, but the Thiele modulus increases with increasing temperature. The Raney nickel grains are too thick and not fully utilized, particularly at high current density.
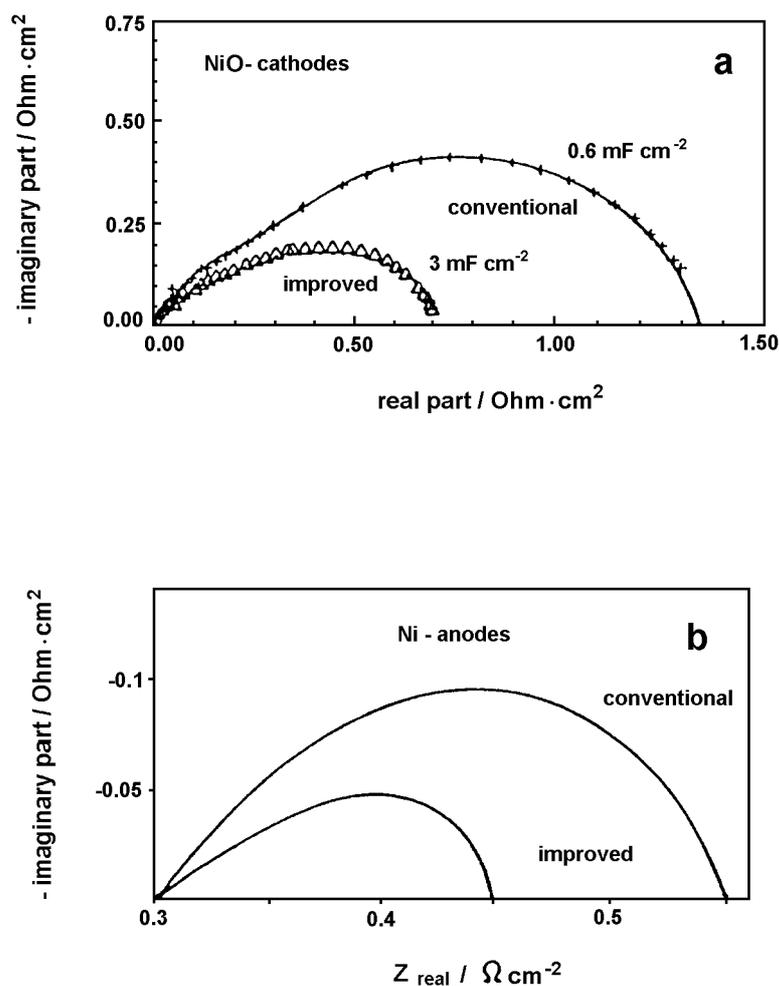
Fig. 33 Nyquist plots of the impedance of anode and cathode (160):
 a.   conventional and improved nickel oxide MCFC cathode
 b.   conventional and improved nickel sponge MCFC anode

Impedance data also showed the improvement of nickel-oxide MCFC cathode and nickel-sponge MCFC anode. The Nyquist plots are shown in Fig. 33.

15.4   Conclusions

EIS is a very attractive and powerful technique in fuel cell research and development. It can be used as an in situ technique and provides kinetic information on the cells. It is also a very powerful means of studying the electrode materials of fuel cells. The interpretation and modeling of EIS data still remain a complex problem, but more detailed development and extended applications of EIS on fuel cell research may be expected in the near future.

References

1. G. Halpert, "Advanced Batteries for Electric Vehicles", in "Proceedings of the Symposium on Electric Vehicles", Edited by S. Surampudi and F. Deligiannis, The Electrochemical Society Inc., (1991).

2. D. R. Squire, "Review of All Solid State Batteries", ibid., (1991).

3. J. R. Selman and Y. P. Lin, "Application of ac Impedance in Fuel Cell Research and Development", in "Second International Symposium on Electrochemical Impedance Spectroscopy", edited by D. D. Macdonald, Electrochimica Acta, 38, 2063 (1993).

4. ZPLOT - electrochemical impedance software, Scribner Associates Inc. (1990)

5. ZPLOT for Windows - electrochemical impedance software, Scribner Associates Inc., (1993).

6. J. R. Macdonald, J. Electroanal. Chem., 307, 1 (1991).

7. F. B. Mansfeld, Tech. Report 026, Solartron, Farnborough, UK (1991)

8. B. A. Boukamp, Equivalent Circuit, University Twente, Report CT89/214/128, The Netherlands (1989).

9. F. B. Mansfeld, H. Shih, and C. H. Tsai, "Software for Simulation and Analysis of Electrochemical Impedance Spectroscopy (EIS) Data", in "Computer Modeling in Corrosion", R. S Munn, Editor, ASTM STP 1154 (1992).

10. F. Mansfeld, H. Shih, H. Greene, and C. H. Tsai, "Analysis of EIS Data for Common Corrosion Porcesses", in "Electrochemical Impedance: Analysis and Interpretation", J. R. Scully, D. C. Silverman, and M. W. Kendig, Editors, ASTM, STP 1188 (1993).

11. D. A. Rand and D. Pavlov, "Proceedings of the International Conference on Lead/Acid Batteries", Drujba, Varna, Bulgaria, May 29-June 2, 1989.

12. R. F. Nelson, "Evolution of Gas-Recombination Lead/Acid Cells and Batteries", ibid.

13. N. E. Bagshaw, "Lead/Acid Recombination Batteries: Principle and Applications", ibid.

14. H. Tuphorn, "Sealed Lead/Acid Batteries: Theory and Applications", ibid.

15. J. A. Magyar, M. A. Kepros, and R. F. Nelson, "Reference-Electrode and Gassing Studies of Lead/Acid Charge-Discharge Processes", ibid.

16. H. Dietz, S. Voss, H. Doring, J. Garche and K. Wiesener, "Measures for Minimizing Hydrogen Pressure in Sealed Lead/Acid Batteries", ibid.

17. W. K. Dimitrov, "Oxygen Evolution on Lead Dioxide in Sulphuric Acid Solutions", ibid.

18.   D. A. Crouch, Jr. and J. W. Reitz, "Relating Recombination Mat Separator Properties to Sealed Lead/Acid Battery Performance", ibid.

19.   E. M. L. Valeriote, J. Sklarchuk, and M. S. Ho, "Corrosion and Growth of Expanded Grids for Maintenance-Free Batteries" in "Proceedings of the Symposium on Advances in Lead-Acid Batteries", edited by K. R. Bullock and D. Pavlov, The Electrochemical Society, Inc., Vol. 84-14, New Orleans, p. 224, 1984.

20.   D. Kelly, P. Niessen, and E. M. L. Valeriote, "The Influence of Composition and Microstructure on the Corrosion Behavior of Pb-Ca-Sn Alloys in Sulfuric Acid Solution, J. Electrochem. Soc. Vol. 132, p. 2533, 1985.

21.   T. G. Chang, "Structural Changes of Positive Active Material in Lead-Acid Batteries in Deep-Discharge Cycling", J. Electrochem. Soc., Vol. 131, p. 1755, 1984.

22.   T. G. Chang and M. M. Wright, "Formation of Trtrabasic Lead Sulfate at Room Temperature", J. Electrochem. Soc., Vol. 128, p. 719, 1981.

23.   E. M. L. Valeriote and L. D. Gallop, "The Kinetics of the Potentiostatic Oxidation of Lead Sulfate Films on Lead in Sulfuric Acid Solution", J. Electrochem. Soc., Vol. 124, p. 370, 1977.

24.   J. Strebe, B. Reichman, B. Mahato, and K. R. Bullock, "Improved Gelled-Electrolyte   Lead/Acid Batteries for Deep-Discharge Applications", J. of Power Source, 31, p. 43, 1990.

25.   B. K. Mahato and W. H. Tiedemann, "Linear Potential Sweep of Lead-Acid Battery Electrodes Containing Trace Te, Sb, As, Co, and Ni", J. Electrochem. Soc., 130, p. 2139, 1983.

26.   B. K. Mahato and J. L. Strebe, "Positive Grid Corrosion in A Deep Discharge Cycled Lead-Acid Battery, Part I: Cycling of Bare Antimonial Grid" in "Proceedings of the Symposium on Advances in Lead-Acid Batteries", edited by K. R. Bullock and D. Pavlov, J. Eelctrochem. Soc. Vol. 84-14, New Orleans, p. 154, 1984.

27.   B. K. Mahato, "mechanism of Capacity Degradation of Lead-Acid Battery", in "Proceedings of the Sixth Annual Battery Conference on Applications and Advances", 1991.

28.   D. Pavlov, "Lead Acid Batteries" in "Power Sources for Electric Vehicles", edited by B. D. MiNicol and D. A. Rand, Elsvier, Amsterdam, 1984.

29.   B. K. Mahato, E. Y. Weissman, and E. C. Larid, "Some Aspects of Gas Recombination in Lead-Acid Systems", J. Electrochem. Soc., 121, p. 13, 1974.

30.   K. R. Bullock, "The Electromotive Force of the Lead-Acid Cell and Its Half-Cell Potential", J. of Power Sources, 35, p. 197, 1991.

31.   W. Peukert, Elekttotech, Z., 18, p. 289, 1897.

32.   G. Liebenow, Z. Electrochem., 4, p.58, 1897.

33.   A. D. Turner and P. T. Moseley, J. Power Sources, 9, p.19, 1983.

34.　D. Linden, "Handbook of Batteries and Fuel Cells", McGraw-Hill, New York, 1984.

35.　L. Fruchter, G. Crepy, and A. LeMehaute, J. Power Sources, 18, p. 51, 1986.

36.　N. F. Compagnone, "A New Equation for the Limiting Capacity of the Lead-Acid Cell", ibid., 35, p. 97, 1991.

37.　N. A. Hampson, S. Kelly, and K. Peters, J. Appl. Electrochem., 11, 751 (1981).

38.　S. G. Canagaratna and H. A. Hampson, J. Electroanal. Chem., 86, 361 (1978).

39.　T. V. Nguyen, R. E. White, and H. Gu, "The Effects of Separator Design on the Discharge Performance of A Starved Lead-Acid Cell", GM Technical Report, GMR-6904, 1990.

40.　A. A. Abdul Azim and K. M. El-Sobki, "Corrosion and Passivity of Pb in Strongly Alkaline Solutions", Corrosion Science, 12, p. 207, 1972.

41.　Y. M. Wang and H. Shih, "Positive Grid Corrosion Evaluation of the Lead Acid Battery by Electrochemical Method", in preparation.

42.　R. Y. Ying, Y. M. Wang, G. C. Garabedian, "Development of An Accelerated Test for Screening Positive Grid Materials Used in the Lead Acid Battery", GM Technical Report PC-658, 1991.

43.　Z. Stoynov, B. Savova-Stoynov, and T. Kossev, "Non-Stationary Impedance Analysis of Lead/Acid Batteries", J. of Power Sources, 30, p. 275, 1990.

44.　P. R. Roberge, E. Halliop, G. Verville, and J. Smit, "Non-Destructive Characterization of Sealed Lead/Acid Battery Cells with Electrochemical Impedance Spectroscopy", J. of Power Sources, 32, p. 262, 1990.

45.　M. Bojinov and B. Monahov, "Impedance Measurements of the Lead/Sodium Sulphate System: Synthesis of AC Analogue Circuit", J. of Power Sources, 30, p.287, 1990.

46.　K. V. Rybalka and L. A. Beketaeva, "Impedance of Porous Electrochemical Systems: Study of the Negative Active Mass of the Lead/Acid Battery", J. of Power Sources, 30, p.269, 1990.

47.　F. Mansfeld, M. Kendig, and S. Tsai, International Congress on Metallic Corrosion, 8th Proc., Mainz, Germany, 1014 (1981).

48.　R. D. Armstrong and K. L. Bladen, J. Appl. Electrochem., 7, 345 (1976).

49.　M. Maja and N. Penazzi, Electrochim. Acta, 30, 773 (1985).

50.　Y. M. Wang, H. Shih, G. Brutchen, and R. Bendert, GM Tecnical Report PC-716 (1992).

51.　Z. Stoynov, B. Savova-Stoynov, and T. Kossev, "Impedance Studies of Inter-Cell Welds in Automotive Lead/Acid Batteries", J. of Power Sources, 30, p.301, 1990.

52.　T. A. Edison, U. S. Pat. 1016874, 1912.

53. R. L. Tichenor, U. S. Pat. 2578027, 1951.

54. A. Dassler, U. S. Pat. 2104973, 1938.

55. A. E. Lange, E. Langguth, E. Breuning, and A. Dassler, U. S. Pat. 2131592, 1938.

56. G. Neumann and U. Gottesmann, U. S. Pat. 2571927, 1951.

57. G. W. Vinal, "Storage Batteries", Wiley, New York, 4th Edn., 1955.

58. O. Jache, U. S. Pat. 3257237, 1966.

59. K. Eberts in D. H. Collins (ed.), Power Sources 2, Pergamon, Oxford, 1970.

60. K. M. Abraham and S. B. Brummer, in Lithium Batteries, J. P. Gabano, Editor, Academic Press, Inc., New York (1983).

61. B. Otzinger, in Proceedings of 1984 GSFC Battery Workshop, NASA conference   publication 2382, p. 95, NASA (1985).

62. S. Subbarao, D. H. Shen, F. Deligiannis, C. K. Huang, and G. Halpert, J. Power Sources, 29, 579 (1990).

63. M. Anderman and J. T. Lundquist, J. Electrochem. Soc., 135, 1167 (1988).

64. A. C. Makrides, K. M. Abraham, G. L. Holleck, T. H. Nyugen, and R. J. Hurd, in Proceedings of the 34th International Power Sources Symposium, Cherry Hill, NJ, June 25-28, 1990, IEEE, p. 167 (1990).

65. S. R. Narayanan, D. H. Shen, S. Surampudi, A. I. Attia, and G. Halpert, J. Electrochem. Soc., 140, 1854 (1993).

66. C. D. Desjardinis, G. K. Mclean, and H. Sharifian, ibid., 136, 345 (1989).

67. N. Takami, T. Ohsaki, and Inada, ibid., 139, 1849 (1992).

68. B. A. Boukamp, "Equivalent Circuit (software for microcomputers)", University Twente, Report CT89/214/128, The Netherlands (1989).

69. B. A. Boukamp, Solid State Ionics, 18, 136 (1986); 20, 31 (1986).

70. G. Montesperelli, P. Nunziante, M. Pasquali, and G. Pistoia, Solid State Ionics, 37, 149 (1990).

71. C. D. Desjardins and K. MacLean, J. Electrochem. Soc., 136, 345 (1989).

72. S. Fouache-Ayoub, M. Garreau, P. V. Prabhu, and J. Thevenin, ibid., 137, 1659 (1990).

73. Y. Matsuda, M. Morita, and S. Aoki, in Rechargeable Lithium Batteries, S. Subbarao, V. R. Koch, B. B. Owens, and W. H. Smyrl, Editors, PV 90-5, p. 67, The Electrochemical Society Softbound Proceedings Series, Pennington, NJ (1990).

74. D. H. Shen, S. Subbarao, F. Deligiannis, C. K. Huang, G. Halpert, and E. Peled, ibid., p. 114.

75. J. Bressan, G. Feuillade, and R. Wiart, J. Electrochem. Soc., 129, 2649 (1982).

76. M. Mogensen, J. Power Sources, 20, 53 (1987).

77. Y. Geronov, B. Puresheva, and B. Pavlova-Stoynov, ibid., 20, 37 (1987).

78. J. Thevenin and R. H. Muller, J. Electrochem. Soc., <u>134</u>, 273 (1987).

79. J. A. Stile and K. Brandt, U. K. Pat. 6B 2105512A (1982).

80. M. Bojinov, Y. Geronov, G. Pistoia, and M. Pasquali, J. Electrochem. Soc., <u>140</u>, 294 (1993).

81. D. P. Wilkinson, H. Blom, K. Brandt, in 5th International Meeting on Li Batteries, Extended Abstracts, p. 56, Beijing, China (1990).

82. K. M. Abraham, J. Power Sources, <u>14</u>, 179 (1985).

83. S. Tobishima, M. Arakawa, T. Hirai, and J. Yamaki, ibid., <u>20</u>, 293 (1987).

84. M. Keddam, O. Matto, and H. Takenouti, J. Electrochem. Soc., <u>128</u>, 257 (1981).

85. O. E. Barcia and O. R. Mattos, Electrochim. Acta, <u>35</u>, 1601 (1990).

86. H. Schweickert, W. J. Lorenz, and H. Friedburg, J. Electrochem. Soc., <u>127</u>, 1673 (1980).

87. A. A. El Milgiy, D. Geana, and W. J. Lorenz, Electrochim. Acta <u>20</u>, 272 (1975).

88. J. .Bessone, L. Karakaya, P. Lorbeer, and W. J. Lorenz, ibid., <u>22</u>, 1147 (1977).

89. P. Lorbeer and W. J. Lorenz, ibid., <u>25</u>, 375 (1980).

90. W. J. Lorenz and F. Mansfeld, in Fundamental Aspects of Corrosion Protection by Surface Modification, Vol. 84-3, p. 144, Electrochemical Society, Princeton, NJ (1984).

91. W. J. Lorenz, 167th Electrochem. Soc., Meet., Toronto, Canada, 1985, paper No. 17.

92. W. J. Lorenz and K. E. Heusler, in Corrosion Mechanisms (F. Mansfeld, ed.). p. 1, Dekker, New York (1986).

93. I. Epelboin, M. Keddam, and H. Takenouti, J. Appl. Electrochem. <u>2</u>, 71 (1972).

94. C. Cachet, B. Saidani, and R. Wiart, Electrochim. Acta, <u>33</u>, 405 (1988).

95. E. Chassaing, M. Joussellin, and R. Wiart, J. Electroanal. Chem. Interfacial Electrochem., <u>157</u>, 75 (1983).

96. H. J. De Wit, C. Wijenberg, and C. Crevecoeur, J. Electrochem. Soc., <u>126</u>, 779 (1979).

97. S. Chechirlian, P. Eichner, M. Keddam, H. Takenouti, and H. Mazille, Electrochim. Acta, <u>35</u>, 1125 (1990).

98. D. D. Macdonald and B. G. Pound, J. Power Sources, <u>29</u>, 477 (1990).

99. J. R. Park and D. D. Macdonald, Corros. Sci. <u>12</u>, 295 (1983).

100. H. T. Taskier, S. M. Mullins, E. A. Langford, and R. J. Fleming, U. S. Pat. 4973532 (1990).

101. J. T. Lundquist, C. B. Lundsager, N. I. Palmer, and H. J. Troffkin, U. S. Pat. 4650730 (1987), and 4,731,304 (1988).

102. A. Yoshino, K. Nakanishi, and A. Ono, Papan Pat. Appl. Tokugan Hei 1-338559 (1989).

103. F. C. Laman, Y. Sakurai, T. Hirai, J. I. Yamaki, and S. I. Tobishima, Extended Abstracts of the 6th IMLB Munster, Germany, May 10-15 (1992).

104. F. C. Laman, M. A. Gee, and J. Denovan, J. Electrochem. Soc., 140, L51 (1993).

105. M .A. Reid, in D. A. Corrigan and A. H. Zinmmerman (eds.), Nickel Hydroxide Electrodes, Proc. Vol. 90-4, The Electrochemical Society, Pennington, NJ, 1990, pp. 296-310.

106. A. H. Zimmerman, M. R. Martinelli, M. C. Janecki and C. C. Badcock, J. Electrochem. Soc., 129, 289 (1982).

107. S. J. Lenhart, D. D. Macdonald, and B. G. Pound, J. Electrochem. Soc., 135, 1063 (1985).

108. R. Haak, C. Ogden, and D. Tench, J. Power Sources, 12, 289 (1984).

109. M. A. Reid, Proc. 25th Intersociety Energy Conversion Engineering Conf., Reno, NV, Vol. 3, p. 48 (1990).

110. H. S. Lim and S. Z. Verwyfelt, J. Power Sources, 22, 213 (1988).

111. H. S. Lim and S. Z. Verwyfelt, ibid., 29, 503 (1990).

112. M. A. Reid and P. L. Loyselle, ibid., 36, 285 (1991).

113. R. D. Armstrong and E. A. Charles, J. Power Sources, 27, 15 (1989).

114. M. A. Reid, J. Power Sources, 29, 467 (1990).

115. W. L. Zhang, M. P. S. Kumar, S. Srinivasan and H. J. Ploehn, J. Electrochem. Soc., 142, 2935 (1995).

116. M. Viitanen, J. Electrochem. Soc., 140, 936 (1993).

117. N. Kuriyama, T. Sakai, H. Miyamura, I. Uehara, H. Ishikawa and T. Iwasaki, J. Electrochem. Soc., 139, 172 (1992).

118. N. Kuriyama, T. Sakai, H. Miyamura, I. Uehara, H. Ishikawa and T. Iwasaki, J. Alloys Comp., 192, 161 (1993).

119. P. Agarwal, M. E. Orazem and A, Hiser, in "Hydrogen Storage Materials, Battery, and Electrochemistry", edited by D. A. Corrigan and S. Srinivasan, The Electrochem. Soc. Proc., PV92-5, 120 (1992)

120. Y. Geronov, B. Puresheva, and B. Pavlova Stoynov, J. Power Sources, 20, 37 (1987).

121. M. Hughes, S. A. G. R. Karunathilaka, N. A. Hampson, and T. J. Sinclair, J. Appl. Electrochem. 12, 537 (1982).

122. J. Harrison, Electrochim. Acta, 28, 1555 (1983).

123. F. Marikar, J. C. Hall, and H. F. Gibbard, "Anode Corrosion in Lithium-Sulfuryl Chloride Batteries".

124. H. Y. Hu and H. W. Ko, J. Power Sources, 26, 419 (1989).

125. Ju. M. Povarov and I. V. Vorobeva, Elecktrokhimiya, 1, 1963 (1982).

126. V. E. Kazarinov and V. S. Bagotzky, J. Power Sources, <u>20</u>, 259 (1987).

127. M. Mogensen, ibid., <u>20</u>, 53 (1987).

128. R. V. Moshtev, Y. Geronov, and B. Puresheva, J. Electrochem. Soc., <u>128</u>, 1851 (1981).

129. J. Jamnik, M. Gaberscek and S. Pejovnik, Electrochimica Acta, <u>35</u>, 423 (1990).

130. M. J. Madou and S. Szpak, J. Electrochem. Soc., <u>131</u>, 2471 (1984).

131. B. R. Karas, J. Electrochem. Soc., <u>132</u>, 1261 (1985).

132. B. R. Karas and R. N. King, ibid., <u>132</u>, 1266 (1985).

133. G. Staikov, P. D. Yankulov, B. S. Savova-Stoynov and Z. B. Stoynov, J. Appl. Electrochem., <u>15</u>, 895 (1985).

134. M. C. M. McKubre, S. I. Smedley and F. L. Tanzella, J. Electrochem. Soc., <u>136</u>, 1969 (1989).

135. P. J. Johnson, J. Power Sources, <u>32</u>, 63 (1990).

136. P. J. Johnson and A. A. Koenig, J. Electrochem. Soc., <u>137</u>, 1121 (1990).

137. J. R. Macdonald and W. B. Johnson, in J. R. Macdonald (ed.), Impedance Spectroscopy, Wiley, New York (1987).

138. J. T. Lundquist, C. B. Lundsager, N. I. Palmer, and H J. Troffkin, U. S. Pat. 4650730 (1987) and 4,731,304 (1988).

139. H. T. Taskier, S. M. Mullins, E. A. Langford, and R. J. Fleming, U. S. Pat. 4973532 (1990).

140. A. Yoshino, K. Nakanishi, and A. Ono, Jpn. Pat. Appl. Tokugan Hei 1-338559 (1989).

141. F. C. Laman, M. A. Gee, and J. Denovan, J. Electrochem. Soc., <u>140</u>, L51 (1993).

142. M. M. Musiani, Electrochim. Acta, <u>35</u>, 1665 (1990).

143. R. W. Murray, in Electroanalytical Chemistry , edited by A. J. Bard, <u>13</u>, 191, Marcel Dekker, New York (1984).

144. T. A. Skotheim (editor), Handbook of Conducting Polymers, Marcel Dekker, New York (1986).

145. R. G. Linford (editor), Electrochemical Science and Technology of Polymers, Vol. 1, Elsevier, London (1987).

146. G. Mengoli, M. M. Musiani, G. Zotti and S. Valcher, J. Electroanal. Chem., <u>202</u>, 217 (1986).

147. D. F. Shriver and G. C. Farrington, Chemical and Engineering News, 42, May 20 (1985).

148. C. Gabrielli, O. Haas and H. Takenouti, J. Appl. Electrochem. <u>17</u>, 82 (1987).

149.T. B. Hunter, P. S. Tyler,W. H. Smyrl and H. S. White, J. Electrochem. Soc., <u>134</u>, 62 (1982).

150. C. Ho, I. D. Raistrick and R. A. Huggins, ibid., <u>127</u>, 343 (1980).

151. C. Doslouis, M. M. Musiani and B. Tribollet, J. Electroanal. Chem., <u>264</u>, 37 (1982).

152. C. Doslouis, C. Gabrielli, P. Sainte-Rose Fanchine and B. Tribollet, J. Electrochem. Soc., <u>129</u>, 107 (1982).

153. T. R. Jow, L. W. Shacklette, M. Maxfield and D. Vernick, J. Electrochem. Soc., <u>134</u>, 1730 (1987).

154. T. F. Otero and E. De Larreta, J. Electroanal. Chem., <u>244</u>, 311 (1988).

155. R. K. Yuan, D. Peramunage and M. Tomkiewicz, J. Electrochem. Soc., <u>134</u>, 886 (1987).

156. T. R. Jow, K. Y. Jen, R. L. Elsenbaumer and L. W. Shacklette, Synth. Metals, <u>14</u>, 53 (1986).

157. S. Cattarin, G. Mengoli, M. M. Musiani and B. Schreck, J. Eelectroanal. Chem., <u>246</u>, 87 (1988).

158. P. G. Bruce and F. Krok, Solid State Ionics, <u>36</u>, 171 (1989).

159. D. Fauteux, ibid., <u>17</u>, 133 (1985).

160. W. Jenseit, O. Bohme, F. U. Leidich, and H. Wendt, Electrochim. Acta, <u>38</u>, 2115 (1993).

161. U. G. Bossel, in Proc. IEA Workshop "SOFC Modeling", Charmey, Switzerland (1989).

162. A. J. Appleby and F. B. Foulkes, Fuel Cell Handbook, Van Nostrand Reinhold Press, New York (1989).

163. K. Kinoshita, F. R. McLarnon and E. J. Cairns, Fuel Cells: A Handbook DOE/METC88/6096, May (1988).

164. R. De Levie, Adv. Electrochem. Eng. <u>6</u>, 329 (1967).

165. T. Springer and I. D. Raistrick, Proc. of the Electrochem. Soc. Symp. on Electrode Materials and Processes for Energy Conversion, Philadelphia, Vol. 87-12, 152 (1987).

166. N. Nicoloso, A. Lobert, W. Weppner and A. Brabenau, Solid State Ionics, <u>44</u>/<u>41</u>, 320 (1990).

167. A. Parthasarathy, C. R. Martin and S. Srinivasan, J. Electrochem. Soc., <u>138</u>, 916 (1992).

168. T. E. Springer, T. A. Zawodzinski, M. S. Wilson and S. Gottesfeld, J. Electrochem. Soc., <u>143</u>, 587 (1996).

169. M. J. Verkerk and A. J. Burggraaf, ibid., <u>130</u>, 78 (1983).

170. A. J. Appleby and S. B. Nicholson, J. Electroanal. Chem., <u>112</u>, 71 (1980).

171. C. Y. Yuh and J. R. Selman, AICHE J. <u>34</u>, 1949 (1988).

172.   T. Nishina and I. Uchida, in Molten Carbonate Fuel Cell Technology, PV 90-16, p. 438, The Electrochem. Society, Pennington, NJ (1990).

173.   T. Nishina, I. Uchida and J. R. Selman, J. Electrochem. Soc., (submitted) (1992).

174. G. L. Lee and J. R. Selman, AC-superimposed-on-DC Characteristics of Fuel Cell electrode Part I & II, J. Electrochem. Soc. (submitted) (1992).

175.   R. Makkus, "Electrochemical Studies on the Oxygen Reduction and NiO(Li) Dissolution in Molten Carbonate Fuel Cells", Doctoral Thesis, Delft University of Technology, Delft, The Netherlands (1991).

176. I. D. Raistrick, Electrochim. Acta, 35, 1579 (1990).

177. T. E. Springer and I. D. Raistrick, J. Electrochem. Soc., 136, 1594 (1989).

178. G. L. Lee and J. R. Selman, AC-superimposed-on-DC Characteristics of Fuel Cell Electrode, submitted to J. Electrochem. Soc. (1992).

179. K. Kordesch, Brennstoffbatterien. Springer, Heidelberg (1985).

180. K. Kordesch, Ber. Bunsenges. Phys. Chem. 94, 902 (1990).

181. P. Stonehart, ibid., 94, 913 (1990).

182. A. Winsel and G. J. Richter, Alkaline Fuel Cells in Electrochemical Hydrogen Technologies, edited by H. Wendt, p. 381, Elsevier, Amsterdam (1991).

183.   F. Mansfeld and W. J. Lorenz, "Electrochemical Impedance Spectorscopy (EIS): Application in Corrosion Science and Technology", edited by R. Varma and J. R. Selman, John Wiley, 581-647 (1991).

184.   W. J. Lorenz, "Dynamic System Analysis and Electrochemical Impedance Spectroscopy in Electrochemistry and Corrosion Science and Technology", classnote at Institute of Physical Chemistry and Electrochemistry, University of Karlsruhe, Karlsruhe, Germany.